Metallic nanoparticle-assisted laser-driven transfer for organic transformations

Inaugural-Dissertation

To obtain the academic degree

Doctor rerum naturalium (Dr. rer. nat.)

submitted to the Department of Biology, Chemistry, Pharmacy

of Freie Universität Berlin

by

Junfang Zhang

from Henan/China

2022

This work was performed between November 2018 and December 2021 under the supervision of Dr. Felix Loeffler and Prof. Dr. Peter H. Seeberger in the Department of Biomolecular Systems, Max Planck Institute of Colloids and Interfaces, Potsdam, and the Institute of Chemistry and Biochemistry, Freie Universität Berlin.

My doctoral degree thesis entitled “Metallic nanoparticle-assisted laser-driven transfer for organic transformations” has been prepared by myself and is based on my own work. This thesis is submitted to the Department of Biology, Chemistry, Pharmacy of Freie Universität Berlin to obtain the academic degree Doctor rerum naturalium (Dr. rer. nat.) and has not been submitted for any other degree.

1st reviewer: Prof. Peter H. Seeberger

2nd reviewer: Prof. Beate Koksch

Date of oral defense: 13.05.2022

Acknowledgement

First, I would like to express my deepest gratitude to Dr. Felix Loeffler for the supervision of my PhD study, for his patience in providing me with suggestions on research, and for his continuous support on this thesis.

I would like to thank Prof. Dr. Peter Seeberger for offering the excellent equipment and working environment in Department of Biomolecular Systems at the Max-Planck-Institute of Colloids and Interfaces and for reviewing this thesis.

I thank Prof. Beate Koksch for kindly agreeing to review this thesis.

I would like to thank all the members of *Synthetic Array Technologies* group and the colleagues of the Biomolecular Systems department. I am very grateful to Dr. Marco Mende, Dr. Yuntao Zhu and Dr. Pietro Dallabernardina for patient training and insightful advice in organic synthesis. I am thankful to Yuxin Liu for fruitful discussion and kind help with scientific art. I would also like to thank Dr. Stephan Eickelmann and Sebastian Ronneberger for the technical help with the laser setup. I am particularly grateful to Dr. Gaofeng Chen for the inspiration of manuscript writing and Giulio Fittolani for beneficial suggestions about sugar chemistry.

My sincere thanks also goes to Eva Settels for her help with the HPLC, to Olaf Niemeyer for the maintenance of NMRs, to Heike Runge, Rona Pitschke, Dr. Tobias Heil, Bolortuya Badamdorj and Dr. Nadja Tarakina for the training and measurement on electron microscopes, to Daniel Werner for the training and maintenance of X-ray diffractograms, to Jessica Brandt for the training and support in electrochemical lab, and to Dr. Oleksandr Savatieiev for the measurement of fluorescence spectrometry.

My deep gratitude also goes to my family and Guangkai for their unconditional love, for supporting me spiritually throughout my Ph.D., for the company and visiting when I am in need, for being my listeners whenever I am emotional, for always being so forgivable when I am unreasonable. I am so lucky to have all of you in my life.

List of Publications

Scientific Publications

1. **Zhang, J**., Liu, Y., Ronneberger, S., Zhao, Z., Seeberger, P. H., Loeffler, F. F., 'Sweet code' - printing sugars for 4D anti-counterfeiting labeling. Manuscript in preparation.
2. **Zhang, J**., Zhu, Y., Njel, C., Liu, Y., Dallabernardina, P., Seeberger, P. H., Savateev, A., Loeffler, F. F., Metal-free photoanode by polymer reactor for C-H functionalization. Manuscript in preparation.
3. **Zhang, J.**,* Liu, Y., Ronneberger, S., Tarakina, N.V., Merbouh, N. and Loeffler, F.F.,* Nanolayer laser absorber for femtoliter chemistry in polymer reactors. *Adv. Mater.*, **2022**, 2108493.
4. **Zhang, J**., Zou, Y., Eickelmann, S., Njel, C., Heil, T., Ronneberger, S., Strauss, V., Seeberger, P. H., Savateev, A., Loeffler, F. F., Laser-driven growth of structurally defined transition metal oxide nanocrystals on carbon nitride photoelectrodes in milliseconds. *Nat. Commun.,* **2021,** *12* (1), 3224.
5. **Zhang, J.,** Gim, S., Paris, G., Dallabernardina, P., Schmitt, C. N. Z., Eickelmann, S., Loeffler, F. F., Ultrasonic-Assisted Synthesis of Highly Defined Silver Nanodimers by Self-Assembly for Improved Surface-Enhanced Raman Spectroscopy. *Chem. Eur. J.,* **2020**, *26* (6), 1243-1248.
6. Eickelmann, S., Ronneberger, S., **Zhang, J**., Paris, G., Loeffler, F. F., Alkanes as Intelligent Surface Thermometers: A Facile Approach to Characterize Short-Lived Temperature Gradients on the Micrometer Scale. *Adv. Mater. Interfaces* **2021,** *8* (3), 2001626.
7. Paris, G., Klinkusch, A., Heidepriem, J., Tsouka, A., **Zhang, J**., Mende, M., Mattes, D. S., Mager, D., Riegler, H., Eickelmann, S., Loeffler, F. F., Laser-induced forward transfer of soft material nanolayers with millisecond pulses shows contact-based material deposition. *Appl. Surf. Sci.,* **2020**, 508, 144973.
8. Eickelmann, S., Tsouka, A., Heidepriem, J., Paris, G., **Zhang, J**., Molinari, V., Mende, M., Loeffler, F. F., A Low-Cost Laser-Based Nano-3D Polymer Printer for Rapid Surface Patterning and Chemical Synthesis of Peptide and Glycan Microarrays. *Adv. Mater. Technol.,* **2019,** *4* (11), 1900503.

Patent Application:

Loeffler, F. F., **Zhang, J.,** Savateev, A., Zhu, Y., Novel carbon nitride compositions and their use as photoelectrodes. EP22151236.1, **2022**.

Scientific Conferences and Symposia Presentations:

January 2022, 5nd International Symposium on Nanoparticles/Nanomaterials and Applications, Lisbon (Portugal), Shotgun presentation

Table of Contents

List of Abbreviations

ACN	acetonitrile
Ar	aryl
aq.	aqueous
BB	building block
BG	band gap
Bn	benzyl
CB	conduction band
CN	carbon nitride
DCM	dichloromethane
DMF	dimethylformamid
DMSO	dimethyl sulfoxide
DP	degree of polymerization
Et	ethyl
EA	electron acceptor
ED	electron donor
EDG	electron donating group
EDX	energy Dispersive X-Ray
EtOAc	ethyl acetate
EPR	electron paramagnetic resonance
e–/h	electron-hole
EWG	electron withdrawing group
FTIR	fourier transform infrared
g-CN	graphitic carbon nitride
HOMO	highest occupied molecular orbital
Hex	hexane
HFIP	hexafluoroisopropanol
HPLC	high performance liquid chromatography
HRMS	high resolution mass spectrometry
HSQC	heteronuclear single quantum coherence spectroscopy
*i*PrOH	isopropanol
LED	light-emitting diode
LUMO	lowest unoccupied molecular orbital
MALDI-TOF	matrix-assisted laser desorption/ionization-time of flight
Me	methyl
MeOH	methanol
MeCN	Acetonitrile
MS	mass spectrometry
NMR	nuclear magnetic resonance
PC	photocatalyst
PG	protecting group

Ph	phenyl
RHE	reversible hydrogen electrode
rt	room temperature
sat.	saturated
SEM	scanning electron microscope
TEM	transmission electron microscope
TFA	trifluoroacetic acid
THF	tetrahydrofurane
THIQ	tetrahydroisoquinoline
TMS	trimethylsilyl
Tol	toluene
UV	ultraviolett
VB	valence band
XPS	X-Ray Photoelectron spectroscopy
XRD	X-ray powder diffraction

Summary

Combinatorial synthesis has emerged as a highly efficient way for the pharmaceutical industry to identify new lead compounds. Recent advances in laser-induced forward transfer (LIFT) show its potential to dramatically miniaturize reaction volumes and precisely deliver different chemical agents in desired positions on a surface, which are crucial steps for combinatorial synthesis. However, the types of molecules which can be delivered by LIFT are limited, resulting in biomolecule microarrays as the core application of LIFT in chemistry. In this thesis, standard polymer-assisted LIFT (polyLIFT) has been further developed to now enable the transfer of a wide scope of materials. More importantly, new applications for this advanced polyLIFT method have been discovered for direct laser-based *in-situ* synthesis.

In Chapter 2, I proposed a hematite nanofilm to replace the traditional (polyimide) laser absorber layer, which revolutionized polyLIFT and enabled many new applications in different fields. For biomolecule coupling reactions, the modified polyLIFT approach exhibited around five times higher spot densities. Moreover, the hematite donor slides showed excellent transfer quality, not only for organic solvent but also water-soluble materials, expanding the achievable reaction types to copper (I)-catalyzed azide-alkyne cycloaddition. Even though employing the hematite nanofilm in LIFT significantly improved the transfer performance, the polyLIFT method was still limited to molecule deposition. Thus, Chapter 3 is focused on the investigation of *in-situ* synthesis through LIFT. Here, another variation of the polyLIFT method, laser-driven transfer synthesis (LTRAS), has been established. During the transfer, a reaction can be simultaneously driven by the laser to generate precisely controlled transition metal oxide nanoparticles on the surface of different substrates within milliseconds. The ability of rapid film functionalization makes LTRAS an efficient strategy for the modification of photoelectrodes. Finally, as a key component of photoelectrochemical (PEC) cells, high-performance photoelectrodes were successfully developed and applied for PEC C-H activation (Chapter 4). A quantitative yield for the oxidation of *N*-aryltetrahydroisoquinolines can be reached without redox mediators, which is not achievable with the gold standard commercially available platinum mesh electrodes. This work offers an environmentally benign and sustainable pathway to synthesize value-added organic compounds by direct usage of solar energy.

In conclusion, the fundamental principles established in this thesis will guide laser-based molecule transfer and synthesis. The presented approach will further encourage

the use of direct-writing techniques in diverse research fields, such as materials science and organic chemistry, and enable many novel applications.

Zusammenfassung

Die kombinatorische Synthese hat sich für die pharmazeutische Industrie als hocheffiziente Methode zur Identifizierung neuer Leitstrukturen erwiesen. Jüngste Fortschritte im Bereich des laserinduzierten Vorwärtstransfers (LIFT) zeigen das Potenzial, Reaktionsvolumina drastisch zu verkleinern und verschiedene chemische Wirkstoffe präzise an die gewünschten Positionen auf einer Oberfläche zu bringen, was für die kombinatorische Synthese entscheidend ist. Die Arten von Molekülen, die durch LIFT übertragen werden können, sind jedoch begrenzt, so dass Biomolekül-Mikroarrays die Hauptanwendung von LIFT in der Chemie darstellen. In dieser Arbeit wurde die standardmäßige polymerunterstützte LIFT (polyLIFT) Methode weiterentwickelt, so dass nun ein breites Spektrum von Materialien übertragen werden kann. Darüber hinaus konnten mit dieser fortschrittlichen polyLIFT-Methode neue Anwendungen für die direkte laserbasierte In-situ-Synthese realisiert werden.

In Kapitel 2 wurde von mir ein Hämatit-Nanofilm als Ersatz für die herkömmliche Laserabsorberschicht (Polyimid) vorgeschlagen, der die polyLIFT-Methode revolutionierte und viele neue Anwendungen in verschiedenen Bereichen ermöglichte. Für Biomolekül-Kopplungsreaktionen wies der modifizierte polyLIFT-Ansatz eine etwa fünfmal höhere Positionsauflösung auf. Darüber hinaus zeigten die Hämatit-Donor-Objektträger eine ausgezeichnete Übertragungsqualität, nicht nur für organische Lösungsmittel, sondern auch für wasserlösliche Materialien, wodurch die mit der Methode möglichen Reaktionstypen auf die Kupfer(I)-katalysierte Azid-Alkin-Cycloaddition erweitert wurden. Obwohl der Einsatz des Hämatit-Nanofilms in LIFT die Übertragsleistung erheblich verbesserte, war die polyLIFT-Methode immer noch auf die Ablagerung von Molekülen beschränkt. Daher konzentriert sich Kapitel 3 auf die Untersuchung der In-situ-Synthese durch LIFT. Hier wurde eine weitere Variante der polyLIFT-Methode, die lasergesteuerte Transfersynthese (LTRAS), entwickelt. Während des Transfers kann gleichzeitig eine Reaktion durch den Laser durchgeführt werden, um innerhalb von Millisekunden präzise kontrollierte Übergangsmetalloxid-Nanopartikel auf der Oberfläche verschiedener Substrate zu erzeugen. Die Fähigkeit zur schnellen Filmfunktionalisierung macht LTRAS zu einer effizienten Strategie für die Modifizierung von Photoelektroden. Schließlich wurden neue Hochleistungs-Photoelektroden als Schlüsselkomponente von photoelektrochemischen (PEC) Zellen erfolgreich entwickelt und für die PEC C-H-Aktivierung eingesetzt (Kapitel 4). Eine quantitative Ausbeute für die Oxidation von N-Aryltetrahydroisochinolinen kann ohne Redox-Mediatoren erreicht werden, was mit dem Goldstandard, den kommerziell erhältlicher Platinnetzelektroden, nicht möglich ist. Diese Arbeit bietet somit einen

umweltfreundlichen und nachhaltigen Weg zur Synthese von schwer zugänglichen organischen Verbindungen durch direkte Nutzung der Sonnenenergie.

Zusammenfassend lässt sich sagen, dass die in dieser Arbeit aufgestellten Grundprinzipien den laserbasierten Molekültransfer mit paralleler Synthese leiten werden. Der vorgestellte Ansatz wird den Einsatz von „direct-write“ Techniken in verschiedenen Forschungsbereichen wie der Materialwissenschaft und der organischen Chemie weiter voranbringen und viele neue Anwendungen ermöglichen.

1. Introduction

1.1. General LIFT process

Direct-writing techniques have been successfully adapted to applications outside the graphics industry, for example, microelectronics and high-density microarrays. Laser-induced forward transfer (LIFT) is one of these direct-writing technologies, which achieves the transfer of materials from a thin film surface onto a receiving substrate. As a maskless and nozzle-free technology, LIFT is highly flexible and efficient for high-resolution printing.

1.1.1. Basic LIFT principles

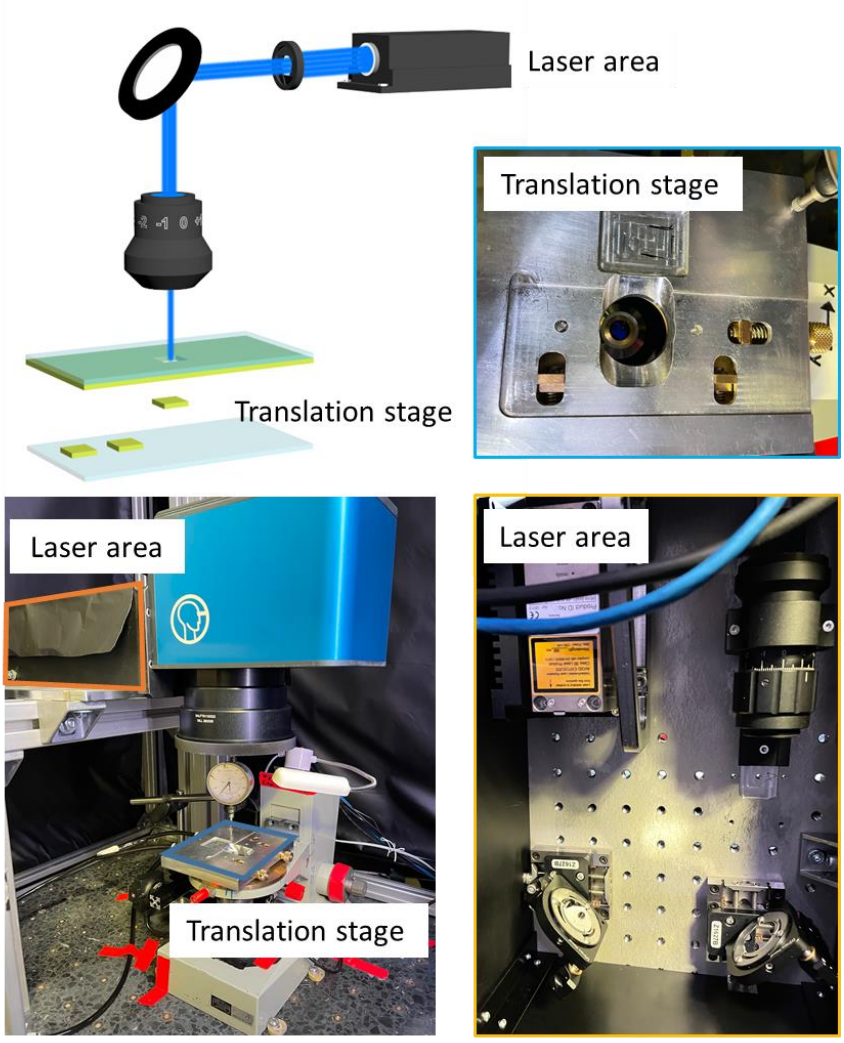

Figure 1-1. Principle of the laser-induced forward transfer (LIFT) process and the laser setup. The laser rapidly heats, melts, and transfers the donor material.

The first report of material deposition using laser sources dates back to the 1970s, while the concept of 'LIFT' was first introduced in 1986 by Bohandy et al.[1] Typically, materials, coated as a solid, liquid or paste layer on the donor substrate, are transferred onto a desired acceptor by a focused laser. The laser passes through the donor substrate and is absorbed by the material layer. The acceptor is in close proximity or in contact with the material film, which can receive the ejected materials under laser irradiation (**Figure 1-1**). LIFT is compatible with a wide variety of substrates for acceptors, including conventional silicon surfaces as well as polymeric foils and paper substrates. Furthermore, the laser and translation stage is normally computer-controlled to achieve rapid motion and required precision for 2D or 3D complex patterns. In general, most of the LIFT processes can be performed under an ambient environment for large area printing.

1.1.2. Variants of LIFT

The great simplicity of the LIFT process gained broad acceptance and has given rise to a large number of variants. Since donor slides, as an essential part of LIFT, highly influence the transfer resolution, here we mainly discuss the LIFT variants based on the differences of donor slides. Donor slides with solid or even liquid films[2] have been reported for the LIFT process. Due to the diverse requirements of transfer applications, several structurally different types of layers for the donor slides have been developed.

1.1.2.1. Transfer with phase change

Typical donors for LIFT are metal-coated slides, which are usually paired with destructive pulsed lasers.[3] The early-stage LIFT process relies on phase transformation of the metal films, which melt, partially vaporize, eject and finally cool down on the acceptor surface. Depending on the donor film thermal diffusion length (L_{th}) and thickness (t), the ejection mechanisms can be either vapor-driven or droplet-mode (**Figure 1-12**). A vapor-driven transfer is observed with thicker donor films ($t > L_{th}$) and shows relatively lower resolution due to the spreading of vapor. Thin donor films ($t \sim L_{\text{th}}$) can be completely melted under laser irradiation. The surface tension and temperature gradients give rise to a jet of molten material, which is observed as droplet-mode LIFT. It achieves high-resolution transfer with spot sizes of a few hundred nanometers. Except for metal layers, semiconductor materials can also be transferred by droplet-mode LIFT, which shows great potential in microelectronics applications. They are mainly suitable for the transfer of robust materials instead of biomolecules or chemicals, due to overheating and/or metal poisoning.

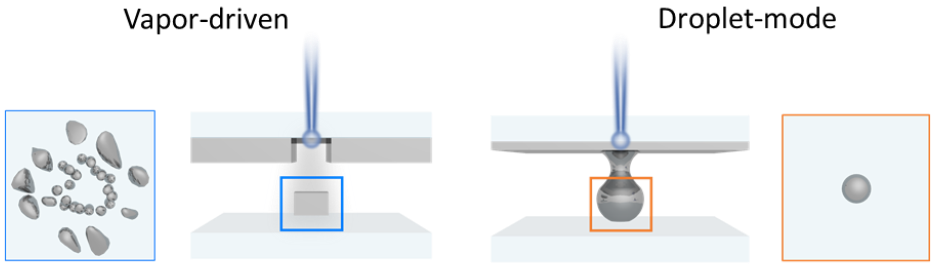

Figure 1-2. Two types of metal transfer by phase-change LIFT process: vapor-driven and droplet-mode.

1.1.2.2. Transfer with intermediate layers

When the donor slides contain pre-structured or sensitive materials, melting or vaporization of the materials can result in the disorder or damage of the material layer. In these cases, introducing intermediate layers help to preserve the desired structure during the transfer. The intermediate, typically a laser absorber layer, is prepared between the donor substrate and material film. A metallic thin film can be the choice of the intermediate layer (**Figure 1-13**). The thickness of the metal films is around 50-100 nm, which is larger than the radiation penetration depth to guarantee that no radiation reaches the material films. The metal layer absorbs the laser radiation, resulting in the vaporization of the underneath material layer. Through bubble expansion and jet formation, materials can be transferred onto acceptor slides. However, vaporization of the material layer is still involved in the LIFT process with metal intermediate layers. They are unable to completely protect the sensitive materials from the heat. Blister-actuated LIFT (BA-LIFT) emerged with a polymer layer (usually polyimide) as the intermediate to solve this problem. Under laser irradiation, the expansion of the polyimide film forms a blister between the donor substrate and the polyimide film, which allows the transfer of the material layer onto acceptors.

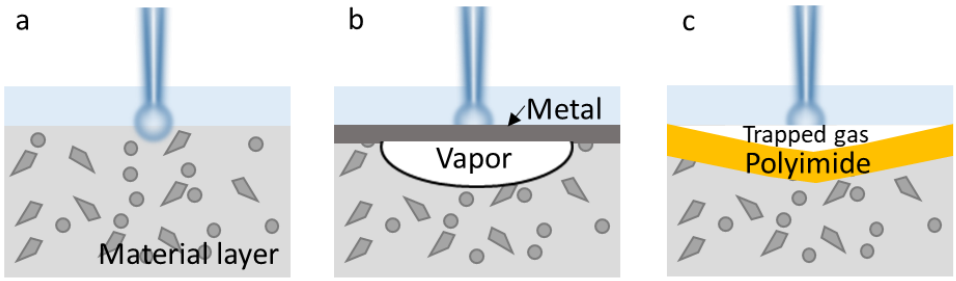

Figure 1-3. Two types of metal transfer by phase-change LIFT process: vapor-driven and droplet-mode. Adapted with permission from Serra *et al*.[4] Copyright (2019).

1.1.2.3. Polymer-based LIFT process

Based on BA-LIFT, a recent variant of LIFT exploits low-cost diode lasers to transfer polymer spots (polyLIFT), which incorporate chemical building blocks. We highlight polyLIFT here since it is the process we are working with in our group. The glass transition temperatures of polymers are typically much lower than the melting or boiling temperatures of metals. Thus, polyLIFT is compatible with less powerful continuous wave lasers. Under laser irradiation, polyimide absorbs the light and converts it to heat. Due to the heat diffusion, the polymer(s) inside the material layer which is in contact with the polyimide film can be warmed up, melted and transferred onto acceptors.

The polymers function as a protective matrix for the chemicals during LIFT, which enables the transfer of fragile chemicals and nanomaterials. The mild transfer conditions and the control over the reaction in polymer reactors, which can be switched on by melting the polymer in an oven, allow for a new approach for chemical reactions. Furthermore, these polymer reactors enable easy control of the spot size for combinatorial chemistry, in comparison with liquid droplets, which have problems of evaporation and diffusion. Nevertheless, the polyimide donor suffers from deformation and degradation (*i.e.*, carbonization) during laser irradiation, which limits its reusability and the resolution of polyLIFT.

1.1.3. Characterization methods of transferred materials

Since the transferred layers by LIFT (especially polyLIFT) are normally very thin, characterization of these thin layers is inevitably challenging. General analysis of layer thickness and morphologies can help us to better understand how different conditions can influence the transfer process. For specific applications, advanced characterization might be needed to show the status of transferred materials, for example, the reactivity of activated molecules or the aggregation of nanoparticles. However, quantitative measurements are in general still unavailable due to the tiny amount of materials transferred. The main idea of microarrays is to use miniaturized high-throughput screening for a qualitative analysis of different biological interactions, chemical reactions, or reaction pathways. Further quantitative analysis of a few positive “hits” from the screening can be performed in larger scale, which highly improves efficiency and reduces workload. Here, I review the technologies commonly used for the characterization of transfer.

1.1.3.1. Vertical scanning interferometry

Vertical scanning interferometry (VSI) performs surface height measurements exploiting the low coherence of white light. Interference will only be achieved when the

path length delays of the interferometer are matched within the coherence time of the light source. VSI is typically used to measure macroscopic objects with surface profiles in the centimeter range. To measure the thickness of multiple spots on one array, the widespread atomic force microscope (AFM) technology can be quite time-consuming, since AFM is not suitable for large areas. Therefore, VSI is the preferred choice for thickness quantification of the LIFT approach.

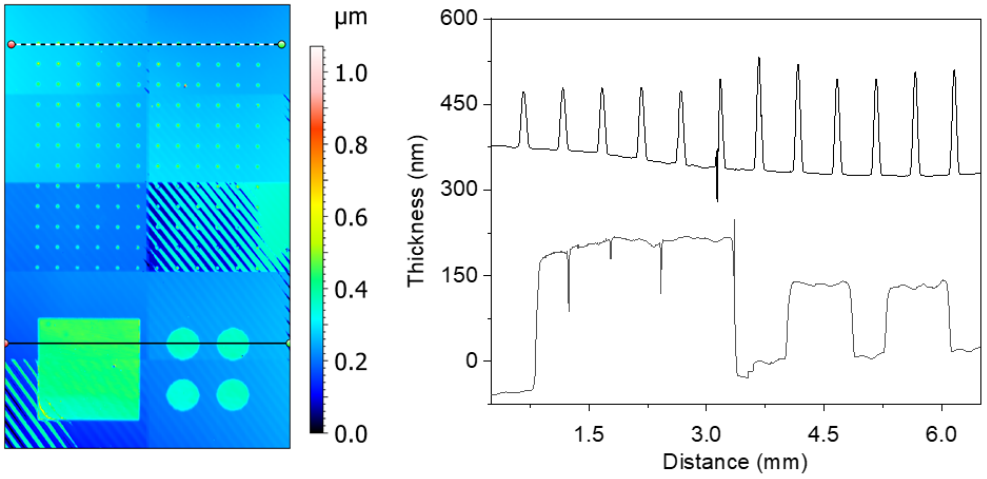

Figure 1-4. Height map and profiles of LIFT transferred spot gradients and areas.

The microscope we are using for VSI is a smartWLI compact (Gesellschaft für Bild- und Signalverarbeitung (GBS) mbH, Illmenau, Germany) with different magnifications (5x, 50x, and 100x Nikon CF IC Epi Plan DI—Mirau). In general, smartWLI provides two data modes of thickness information (**Figure 1-14**): color map and profiles. For a color map, the material distribution and surface roughness of the transferred layer can be clearly observed, while for profiles, the detailed information, for example, the spot height, can be precisely readout down to nanometer precision. Interference wave patterns on the color map sometimes unexpectedly appear due to the method, but this generally does not influence the thickness information. The supporting software MountainsMap 8.0 allows further analysis for spot volumes. We set a threshold which is the upper limit of the substrate surface for the spot array, the thickness and area of each spot will be measured and integrated into the spot volumes (**Figure 1-15**).

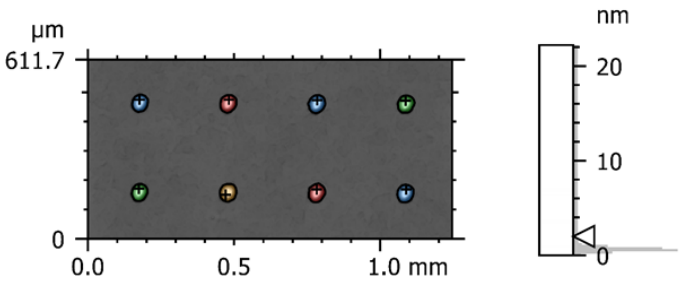

Information		
Method	Threshold detection	
Threshold 1	1.752	nm

Parameters	△ Volume	Z-mean
Unit	nm³	nm
Particle #1	2.506912699e+10	11.18
Particle #2	2.593230589e+10	11.05
Particle #3	2.591761331e+10	10.67
Particle #4	2.537137692e+10	10.72
Particle #5	2.625760667e+10	10.63
Particle #6	2.517984262e+10	11.33
Particle #7	2.606944399e+10	10.74
Particle #8	2.647885318e+10	11.04
Mean	2.57845212e+10	10.92

Figure 1-5. Volume measurement of a spot array by a threshold detection method.

1.1.3.2. Fluorescence scanning

Fluorescence scanning is another important way for the characterization of transferred materials, especially for biomedical applications. It is extremely sensitive, rapid, and comparatively inexpensive. The main drawback of fluorescence scanning is that it usually requires the use of a label, which may possibly interfere with the binding event on the microarray surface. Especially when the native structure of the analyte molecule has not yet been fully established, false-positive or false-negative results can be observed. However, this can be solved by attaching the label onto non-functional sites, for example, serine or cysteine residues of proteins.[5] The choice of dye is frequently dominated by the optical setup and the type of experiment performed. Typical examples for popular fluorophores include reactive dyes for the labeling of peptides, proteins and (oligo)nucleotides; fluorescent proteins for cell studies; fluorophore-labeled biomolecules such as secondary antibodies for immunohistochemistry and flow cytometry; as well as DNA hybridization probes and contrast agents for *in vivo* NIR fluorescence imaging of pathological changes.[6]

Based on the general fluorescence spectroscopy guidelines, plenty of factors can influence the quality of microarray imaging. One of the most important parameters for comparing fluorophores is the fluorescence quantum yield (Φ_f), which is defined as the ratio of the number of photons emitted to the number of photons absorbed. The product of Φ_f and the molar absorption coefficient at the excitation wavelength ($\varepsilon(\lambda_{ex})$) gives the fluorophore's brightness B ($B = \Phi_f \times \varepsilon(\lambda_{ex})$), which determines the analytical sensitivity from the fluorophore side.[7] Values of brightness B below 5,000 render a label for practical use. Another important area for scanning quality is the fluorescence detector. The commercialized electron-multiplying CCD chips allow for low-level and single-molecule detections for microarrays.[8]

1.1.3.3. Mass spectrometry

Detection of microarray binding can also be done using mass spectrometry (MS). Recently, matrix-assisted laser desorption/ionization (MALDI) MS has emerged as a label-free analytical tool for quantitative scanning. Specifically, in cell-based drug discovery and profiling, with the advantages of molecular specificity and fast scanning speed, MALDI-MS has the possibility to be the leading technology for the detection of multiple analytes in parallel. However, MALDI–MS requires conductive and laser-compatible sample plates for high ion yield and strong signal readout. Therefore, a specialized platform is needed to detect the biomolecules of intact treated cells directly. Levkin et al. developed a miniaturized cell screening platform based on arrays of well-separated hydrophilic droplets for monitoring the intracellular accumulation of malonyl-CoA in live cells (**Figure 1-16**).

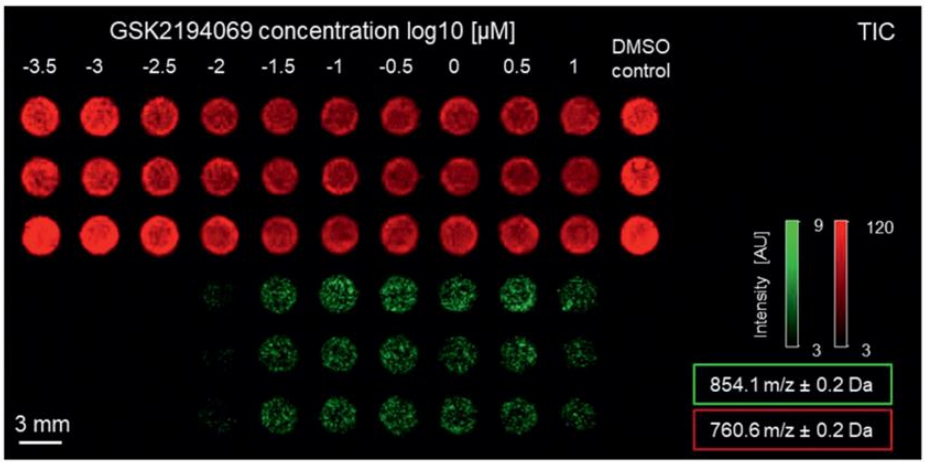

Figure 1-6. Quantitative analysis of the GSK20194069 drug response in live cells on the cell screening platform. Adapted with permission from RamalloGuevara *et al*.[9] Copyright (2021).

1.2. LIFT in materials science

1.2.1. Microelectronics

Printed electronics, for example, organic thin-film transistors (OTFTs) and micro-capacitors, are one of the most important applications of LIFT in materials science. To build a well-functioning electronic device, we need to stack different conducting, semiconducting and insulating layers in a particular configuration. Although plenty of direct-writing methods can be used for the preparation of electronics, solvent compatibility between adjacent layers makes it a big challenge to generate multilayer structures. In the LIFT process, high viscosity liquid donors and even solid donors can be used for printing, which overcomes those difficulties. By designing donor slides with multiple layers, devices can be achieved in a single transfer. Since most light-emitting polymers (LEPs) are sensitive to light, another problem for LIFT is to preserve the structure and properties of the films under optical and thermal treatment from laser irradiation. Therefore, an intermediate layer is necessary to protect the active materials.

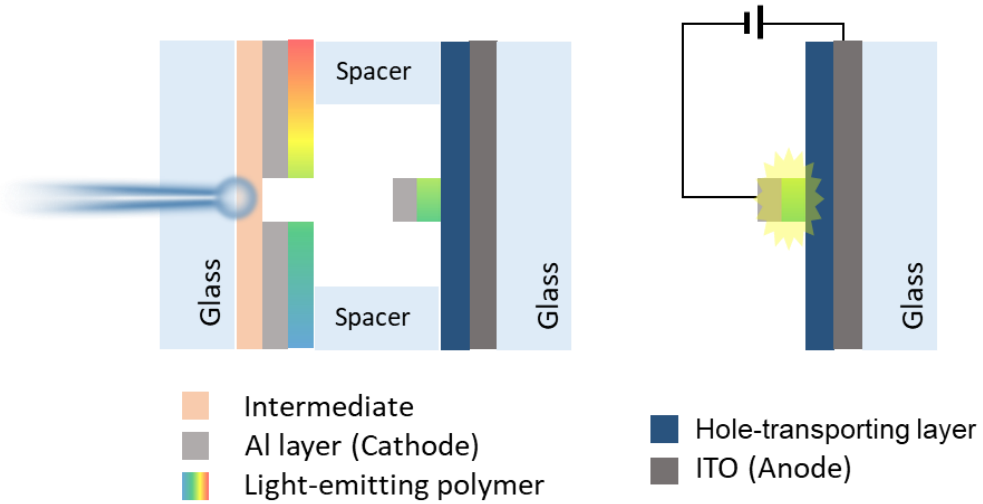

Figure 1-7. LIFT printed organic light-emitting diode with detailed structure of donor and acceptor slides. Adapted with permission from Serra *et al*.[4] Copyright (2019).

One example can be the LIFT printed organic light-emitting diode (OLED) from Nuesch et al. (**Figure 1-17**).[10] For donor slides, they used a thin triazene polymer layer (TP) as an intermediate. An aluminum cathode and the light-emitting polymer (LEP) layer are placed on top of the intermediate as material layers. Under UV laser irradiation, the TP layer decomposes and propels the material layers to the acceptor, which is an indium-doped tin oxide (ITO) glass coated with hole-transporting layers (HTLs). A well-defined gap is introduced between the donor and acceptor for a faster turnover of the acceptor. By using different light-emitting polymers on the donor slides, three colored pixels with

a size of 20 µm are obtained by the LIFT process, providing the possibility to generate high-definition displays.

1.2.2. 3D micro-printing

Microfabrication processes capable of generating 3D structures of different materials have attracted wide attention. During the last five decades, the development of microfabrication technologies achieves progressively higher levels of integrated circuits and microfluidic devices.[11] However, most of these technologies, including soft lithography, localized electrochemical deposition and ink-jetting, focus on 2D microfabrication and are not compatible to build entire 3D microstructures. Another way will be scaling a given macro-scale 3D printing process down to smaller dimensions. However, difficulties like resolution limitation and removal of the final microstructure from substrates without damage, are encountered.

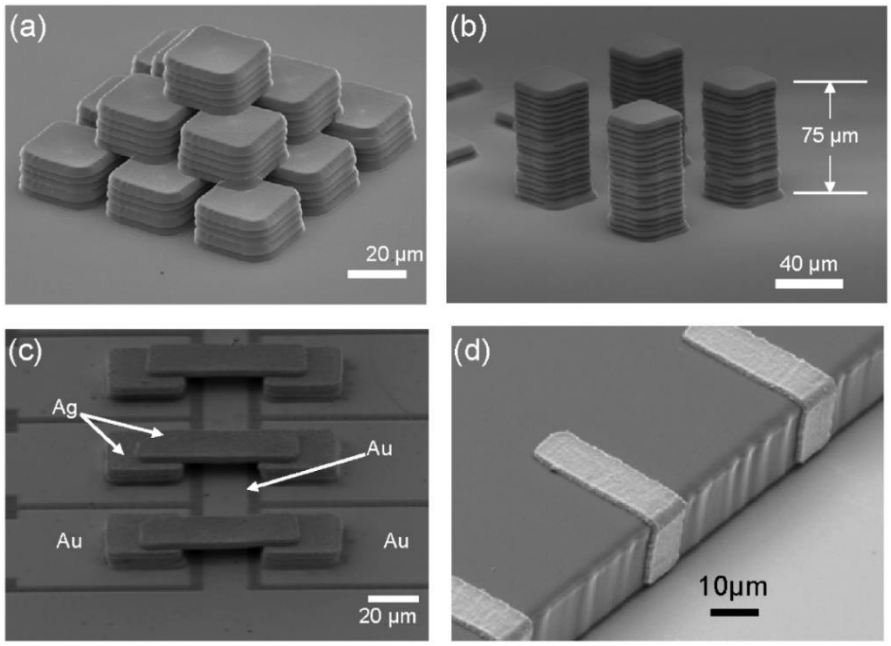

Figure 1-8. SEM images of 3D microfabricated structures achieved by LIFT. (a) (b) Printed vertical interconnects generated by repeated transfers over the same region on acceptors. (c) Free-standing cross-overs made by combinatorial LIFT printing. (d) Folded interconnects over the edges of steps. Adapted with permission from Serra *et al*.[4] Copyright (2019).

LIFT can be applied for 3D microfabrication due to its ability to generate free-standing structures (**Figure 1-1)**. Besides the general 3D layer-by-layer structure, cross-over and folded interconnects can also be obtained by the LIFT process.[12] The transfer process is repeated over the same position to stack the desired out-of-plane structures.

Therefore, the adhesion between different layers should be strong enough to withstand mechanical and thermal strains during the repeating process. In this case, a spacer between the donor and the acceptor can be introduced. When the space becomes larger, the accuracy of transfer tends to decrease. A suitable spacer is critical to find the balance between the stability of the microstructure and transfer accuracy. Moreover, preparing material by nano-suspensions instead of large particles shows better adhesion between the transferred layers. Another challenge is the possible oxidation of materials during the transfer process. Previous results indicate that operating at high fluences (above threshold) and ultra-short laser pulses (picoseconds) can speed up the solidification of the drops during LIFT and minimize oxidation.[13]

1.2.3. Power storage

Due to the ability to deliver pulsed power and provide load leveling, high-performance capacitors are a key component for diverse energy storage systems. Recently, autonomous microelectronic systems obtained widespread attention which brings the need for micro-power sources with high energy density. With the LIFT process, one can not only build microscale devices, but also form porous structures with high surface area. These porous structures are in fact beneficial for energy storage. The increased contact area between the electrodes and the electrolyte leads to more efficient charge transfer and delivery. Therefore, the LIFT process can be used to print micro-ultracapacitors and micro-batteries.

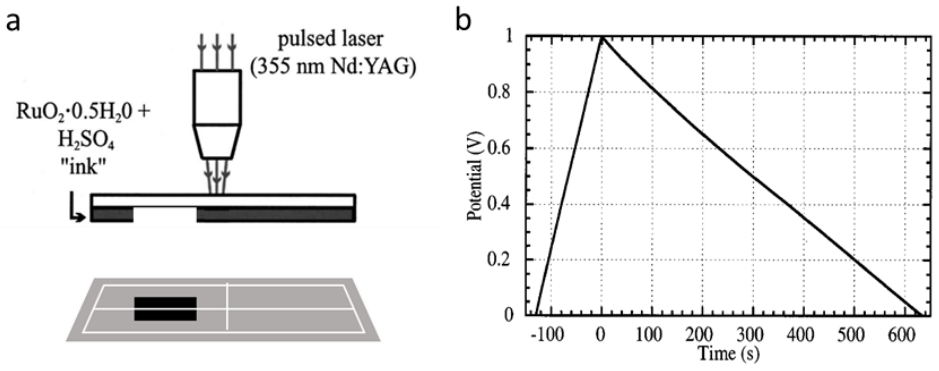

Figure 1-9. Principle of the laser-induced forward transfer (LIFT) process for the generation of micro-ultracapacitor. (a) The electrode material, hydrous ruthenium oxide and electrolyte H_2SO_4, are premixed as the ink to prepare the donor slide. The acceptor is a gold-coated quartz wafer with a 'windowpane'' structure to electrically isolate four current collector pads. (b) Chronopotentiometry from a single micro-ultracapacitor cell charged at 50 µA and discharged at 10 µA. Adapted with permission from Arnold *et al*.[14] Copyright (2003).

In the most straightforward form, a micro-ultracapacitor can be constructed of two identical electrodes separated by an appropriate electrolyte. The possible sources for charge storage in these devices are the electrostatic double-layer effect between electrodes and electrolyte in typical capacitors and Faradaic transfer at the surface of electrodes. In either case, electrodes play an important role in the whole performance of the micro-ultracapacitor. Due to the high specific capacitance (capacitance per unit mass), hydrous ruthenium oxide is considered as ideal electrode material for micro-ultracapacitor. However, the generation of hydrous ruthenium oxide thin films is a quite challenging subject due to the process temperature/pressure limitations. Well-known thin film technologies such as physical or chemical vapor deposition can make the material lose its structural water in the lattice, which provides nanostructured percolation pathways for proton conduction.

Arnold et al. overcome these difficulties by using the LIFT process for the deposition of hydrous ruthenium oxide to prepare micro-ultracapacitors (**Figure 1-1**).[14] The ability to deposit the electrolyte (liquid sulfuric acid) with the electrode material ($RuO_2 \cdot 0.5H_2O$) is an attractive aspect of the LIFT process. The acceptor slide is pre-coated with a gold layer to make it conductive. A 'windowpane'' structure by laser ablation isolates the gold layer into four current collector pads. Two thick lines of hydrous ruthenium oxide are deposited across the groove on a gold layer to establish a symmetric planar micro-capacitor. At a constant charging current of 50 μA and a discharge current of 10 μA, the chronopotentiometry of a single micro-ultracapacitor cell shows ideal linear behavior. The specific capacitance is determined by normalizing the actual capacitance by the experimentally measured mass of the deposited material, yielding 80±2.5 F/g. This value of micro-capacitor is comparable to the reported large-size hydrous ruthenium oxide ultracapacitors.

1.3. LIFT in synthetic chemistry

1.3.1. Biomolecule microarrays

Biomolecules are highly selective sensing agents, therefore, they are the essential component in biosensors, microarray chips, and wearable diagnostic kits. Irrespective of their particular principle of operation, all these devices rely on the deposition and immobilization of one or more different types of biomolecules on specific substrates. Furthermore, the miniaturization of these devices allows the parallel detection of thousands of different biomolecules in genomics and proteomics applications. Combinatorial synthesis of oligo- and macromolecules (*e.g.*, peptides or DNA) on surfaces offers an efficient way for the generation of these devices since it can save significant resources in regard to processing time and material use. Currently, SPOT

synthesis and photolithography are the widely used methods for the synthesis of biomolecule microarrays. However, the limited resolution by liquid diffusion or the low yield due to photochemical protection makes them inappropriate for rapid prototyping applications and customized needs.

Although LIFT was initially developed to transfer metals, its use was quickly extended to oxides and other inorganic materials. The high spatial resolution of LIFT makes it competitive in front of other more conventional techniques. Since biomolecules can be easily decomposed or altered by high temperature, matrix-assisted pulsed-laser evaporation direct-write (MAPLE-DW) was proposed as a solution of such delicate materials,[15] which is in fact one variation of LIFT. In this case, the materials are embedded in a polymer matrix on the donor slides. During the transfer process, the polymer matrix absorbs laser radiation and decomposes, protecting the biomolecules inside, which arrive at the surface of acceptors without damage.[14] Colina et al. demonstrated that DNA can be successfully deposited by the LIFT process without loss of bioactivity.[16] Loeffler et al. reported the consecutive deposition of reagents and amino acids embedded in polymers for in-situ activation of building blocks. [17] Moreover, bovine serum albumin (BSA) is the first protein that has been successfully printed by LIFT.[18] After that, LIFT has proven the feasibility for printing diverse biomolecules like antigens,[19] immunoglobulins,[20] enzymes,[21] and horseradish peroxidase.[22]

1.3.2. Chemical sensors

During the last ten years, LIFT technologies have progressed not only in simple electronics but also in chemical sensors, which show a growing need for advanced integration complexity with reduced component size. The principle of sensors is that the sensing element can reversibly and selectively react with the analyte and release detectable signals. Chemical sensors are typically used for the detection of various gases or vapor molecules. Based on different transducing mechanisms, such as, resistive,[23] capacitive,[24] surface acoustic wave,[25] and film bulk acoustic resonators,[26] LIFT shows its possibility for a wide range of chemical sensors. More interestingly, due to the high spatial resolution of LIFT, this technology can actually generate chemical sensor arrays with hundreds of sensing sites.[24, 25] One of the most important factors that determine the quality of a sensor array is the minimization of cross-talk between adjacent sensors. The ability of non-contact transfer from solid-phase donors makes LIFT a competitive technology for the fabrication of sensor arrays. Furthermore, LIFT can be used not only as a stand-alone deposition technique but also as complementary to other laser processes, presenting unique advantages in modern integrated sensing processing.

Tsouti *et al.* reported a capacitive chemical sensor array with 256 sensing sites for the detection of methanol, water and ethanol vapors (**Figure 1-110**).[24] Each sensor in the array is composed of a Si membrane, which is supported onto a thick SiO_2 layer with a circular cavity underneath. They used LIFT technology to deposit a sensitive polymer layer on the Si membrane, forming the basic sensing element. When the sensor is exposed to the analyte, the polymer layer absorbs the corresponding vapor molecules, swells and its mechanical properties change, resulting in a change of the membrane deflection. Therefore, when the membrane and counter electrode is connected into a circuit, the change of capacitance signal can be observed. Since each sensor membrane is covered by a different sensitive polymer, it is possible to obtain the "signature" of complex odors and eventually arrive at effective odor identification.

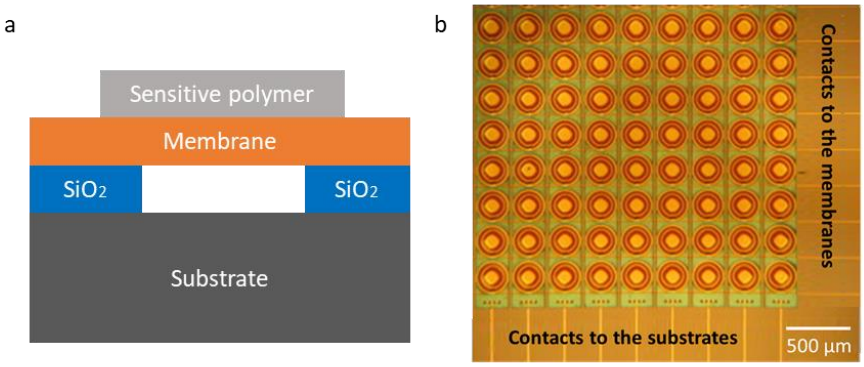

Figure 1-10. A capacitive chemical sensor array with multi sensing sites for the detection of methanol, water and ethanol vapors. (a) Schematic of the polymer/membrane sensor structure. (b) Optical microscopy images of the sensor array. Adapted with permission from Tsouti *et al*.[24] Copyright (2010).

1.4. Aims of this thesis

The general aim of this thesis was 1) the development of an efficient synthetic strategy to produce microarrays, which will be further used for 2) functionalizing photoelectrodes and 3) optimizing conditions for organic transformations by high-throughput screening.

In more detail, the first aim of the thesis was to optimize the polyLIFT process by introducing advanced donor slides. The new donor slides need to:

- ensure high laser absorption and heat stability;
- improve the transfer resolution and efficiency;
- be wettable by multiple solvents and compatible with a wide scope of polymer matrices;

- be able to heal and reuse the polymer films with simple treatments.

The second aim of this thesis was to explore new applications of the polyLIFT process. The LIFT technology has been established more than 30 years ago, however, the main goal of LIFT is still precise deposition of materials. We try to design a variant that enables *in-situ* synthesis of nanoparticles to functionalize acceptor films. Through parameter scanning, the obtained films can be used for the design of photoelectrodes. This task can be separated into the following steps:

- We need to understand how different factors influence the morphologies of nanoparticles. To do that, a collection of nanoparticles needs to be synthesized.
- Thermal characterization of the laser process has to be performed to discover how laser parameters change the synthesis conditions.
- The obtained particles need to be analyzed in terms of structures and photoelectrochemical properties. The mechanism should be further revealed.
- Photoelectrodes with improved performance can be designed.

The third aim of this thesis was to generate and study photoelectrodes for practical organic transformations. To this end:

- The energy structure of photoelectrodes needs to be further designed for efficient charge transfer.
- The current densities of photoelectrodes have to be analyzed for different electrolytes.
- The redox potential of the desired reactions should be investigated.
- The reaction conditions need to be optimized and the scope of substrates should be investigated.

2. Nanolayer laser absorber for femtoliter chemistry in polymer reactors

This chapter has been modified in part from the following article:

J. Zhang, Y. Liu, S. Ronneberger, N. V. Tarakina, N. Merbouh, and F. F. Loeffler, Nanolayer laser absorber for femtoliter chemistry in polymer reactors. *Adv. Mater.,* **2022**, 34, 2108493.

3. Modification of photoanodes by forming heterojunctions with metal oxides

This chapter has been modified in part from the following articles:

Zhang, J.; Gim, S.; Paris, G.; Dallabernardina, P.; Schmitt, C. N. Z.; Eickelmann, S.; Loeffler, F. F., Ultrasonic-Assisted Synthesis of Highly Defined Silver Nanodimers by Self-Assembly for Improved Surface-Enhanced Raman Spectroscopy. *Chem. Eur. J.,* **2020**, *26* (6), 1243-1248.
https://doi.org/10.1002/chem.201904518

Zhang, J.; Zou, Y.; Eickelmann, S.; Njel, C.; Heil, T.; Ronneberger, S.; Strauss, V.; Seeberger, P. H.; Savateev, A.; Loeffler, F. F., Laser-driven growth of structurally defined transition metal oxide nanocrystals on carbon nitride photoelectrodes in milliseconds. *Nat. Commun*., **2021**, 12 (1), 3224.
https://doi.org/10.1038/s41467-021-23367-7

The chapter has been removed for copyright reasons in the online version. For more information about this chapter, please check the above publications.

4. Metal-free photoanodes for organic transformation

This chapter has been modified in part from the following manuscript (in preparation) and a filed patent application:

Zhang, J.; Zhu, Y.; Njel, C.; Liu, Y.; Dallabernardina, P.; Seeberger, P. H.; Savateev, A.; Loeffler, F. F., Metal-free photoanode by polymer reactor for C-H functionalization. Manuscript in preparation.

Loeffler, F. F., **Zhang, J.,** Savateev, A., Zhu, Y., Novel carbon nitride compositions and their use as photoelectrodes. EP22151236.1, **2022**.

4.1. Introduction

Photoelectrochemistry (PEC) provides an environmentally benign and sustainable pathway for the direct conversion of solar energy into the thermodynamic potential that may be used for water splitting, synthesis of chemical fuels and value-added organic compounds. The potentials of the valence band (VB) of the photoanode and of the conduction band (CB) of the photocathode define oxidation and reduction power accessible for a given semiconductor upon excitation with light. This chapter focuses on the synthesis of high-performance of metal-free photoanodes and PEC oxidation half-reaction. In PEC, bias voltage facilitates separation of photogenerated charges and can be used to enable challenging reactions at the cathode.

Preparing photoelectrodes that can work effectively in non-aqueous media for organic transformations is a technical challenge. As the key component of PEC cells, photoelectrodes utilize solar energy to generate, separate, and transport charge carriers. State-of-the-art photoanodes are mainly based on metal oxides, such as $BiVO_4$, WO_3, and α-Fe_2O_3. Under visible light irradiation, they can achieve comparable conversion rates as commercially available platinum or glassy carbon electrodes, with even lower applied potentials. When PEC cells are used to perform organic transformations, superior selectivity can be achieved when using engineered photoanodes compared to only photoredox or electrochemical methods, highlighting PEC cells as an attractive approach for organic transformations. However, PEC properties of most electrodes decrease in non-aqueous electrolytes. Meanwhile, metal-free photoanodes are rarely reported for organic transformations due to their poor PEC properties.

Carbon nitrides (CN) have received wide attention as photocatalysts thanks to their defective graphene-like structure. The main limitations, hindering CN as electrode materials, are their poor electrical conductivity and fast charge recombination. A balance between electrical properties and reactivity is difficult to achieve. For instance, while eliminating nitrogen by high temperature can improve the conductivity of CN, it also results in the loss of redox-active centers. In addition, interfacial resistance between the conductive support (e.g. FTO) and CN disfavors charge transport. Therefore, the preparation method for CN is fundamental in obtaining a material with desired properties and unconventional preparation approaches of CN photoelectrodes are required to prepare high-performing and stable photoanodes.

Here, we report kinetic carbon nitride (kCN) electrodes with a double-layer structure that show unprecedentedly high photocurrents of 975 µA cm^{-2} (**Figure 4-1**). The kCN electrodes are prepared through co-condensation in polymer reactors combined with a chemical vapor deposition (CVD) process. The polymer serves as a sacrificial template that facilitates growth of kCN on the surface of the substrate and it is eliminated gradually at the end of the synthesis. For the first time, this metal-free kCN photoanode was applied to a C-H functionalization, giving a drastically improved yield when compared to a standard Pt working electrode.

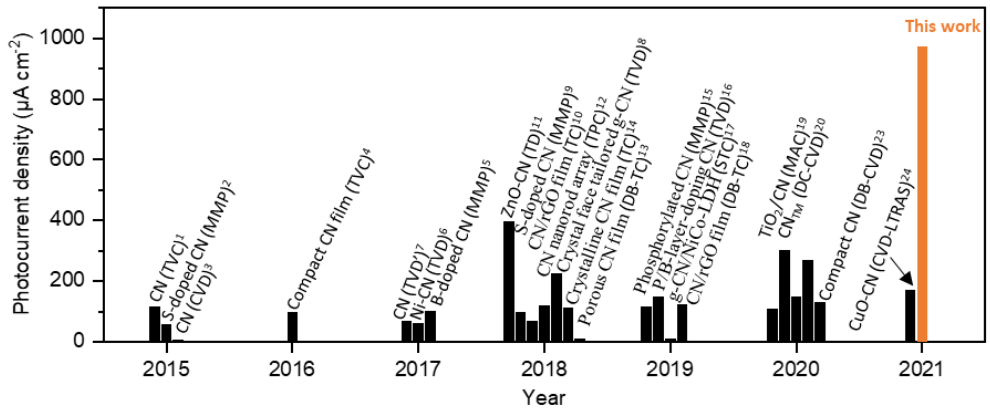

Figure 4-1. Overview of state-of-the-art CN-based photoanodes.

4.2. Results

4.2.1. Photoanode synthesis and molecular structure

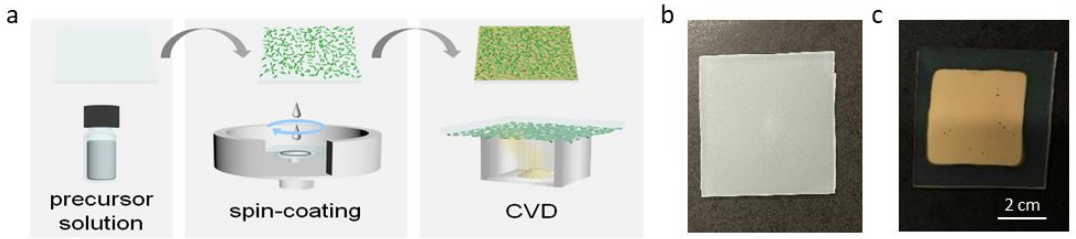

Figure 4-2. (a) Synthesis process of the photoanodes. Photographs of the films (b) after spin coating, (c) after chemical vapor deposition (CVD).

For the synthesis process, a polymer film is introduced by a spin-coating pretreatment step. Carbon nitride precursors and a polymer, typically polystyrene (PS), are dissolved in a solvent and spin-coated, to form a homogeneous film on a conductive substrate. Here, the polymer functions as a film-forming agent. While many precursors are typically not soluble in common solvents, the polymer matrix enables the preparation of a homogenously distributed film (**Figure 4-2**).

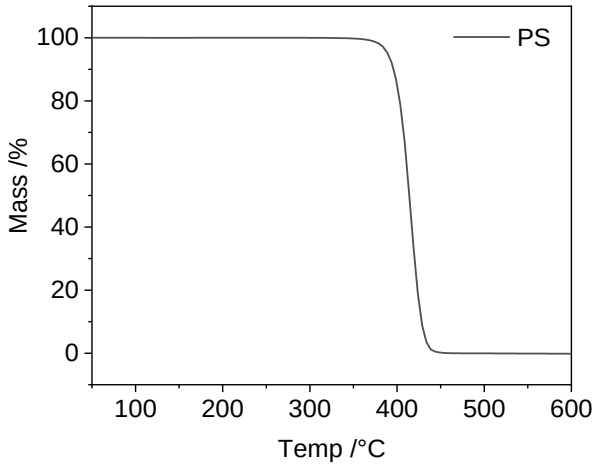

Figure 4-3. Thermogravimetric analysis of polystyrene (PS).

Afterwards, the pretreated substrates undergo a CVD process to give the final electrodes. In this step, the state of the polymer matrix changes continuously along with the increase in temperature. Melting occurs at the glass transition temperature of 67.2 °C, followed by decomposition at around 400 °C and formation of a residual carbon skeleton (**Figure 4-3**). When the temperature surpasses 500 °C, the carbon skeleton gradually disappears (**Figure 4-4a**). As the electrodes are synthesized in this kinetically changing polymer, we call it kinetic carbon nitride (kCN). As a reference, we

deposited a carbon nitride thin film on the surface of FTO substrate by CVD without pre-treatment, to compare its performance with our kCN electrodes. In the infrared spectrum (**Figure 4-5**), kCN presents similar characteristics to CN films, suggesting a retention of the heptazine rings. The main difference is the decreasing intensity of the N-H stretching peaks between 3000 and 3500 cm-1, suggesting a higher polymerization degree in kCN. X-ray photoelectron spectroscopy (XPS) analysis exhibits, after surface cleaning, the ratio between sp2 C and N in heptazine rings is close to 0.75, which is the theoretical maximum for perfectly polymerized carbon nitride (**Figure 4-4b**). The defined area inside mesoporous reactors and higher pressure caused by the vapor influence the growth of carbon nitride. This may explain the higher polymerization degree than typical synthesis approaches. Additionally, in the high-resolution XPS C1s spectrum, the peak is located at 285 eV, which corresponds to C-C bonding, which can still be observed, even after 5 h of surface etching (**Figure 4-4c**). These results indicate that two types of nitrogen defects (i.e., reduced terminal -NH_2 and introduced C-C) arise in the CN framework. In other words, the polymer may function as a sacrificial template that directs growth of the final carbon nitride thin film.

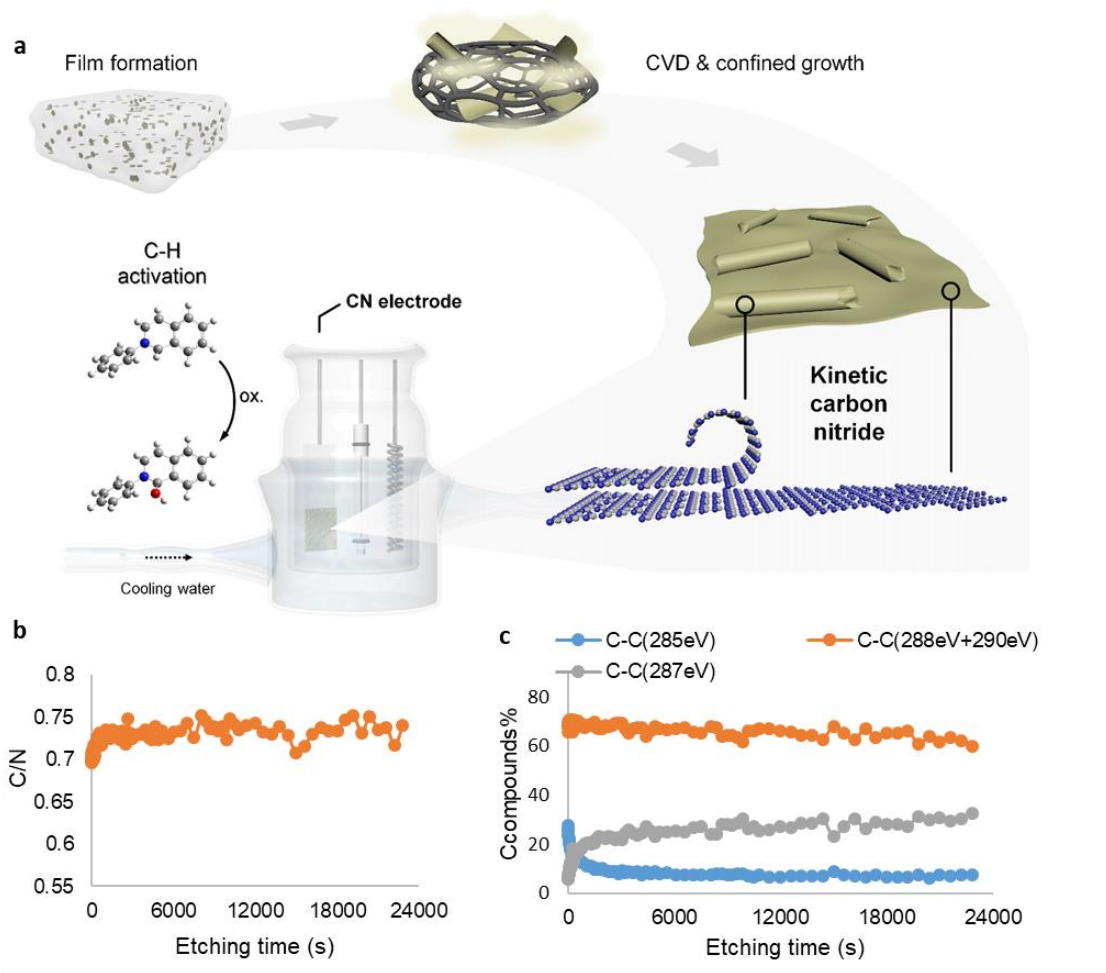

Figure 4-4. Photoanode synthesis and molecular structure. (a) Synthesis of kinetic carbon nitride (kCN) in the polymer film. (b) XPS depth profile of the ratio between carbon and nitrogen under Argon cluster ion etching (6 keV Ar_{1000}^{+}). (c) High-resolution XPS C 1s spectrum.

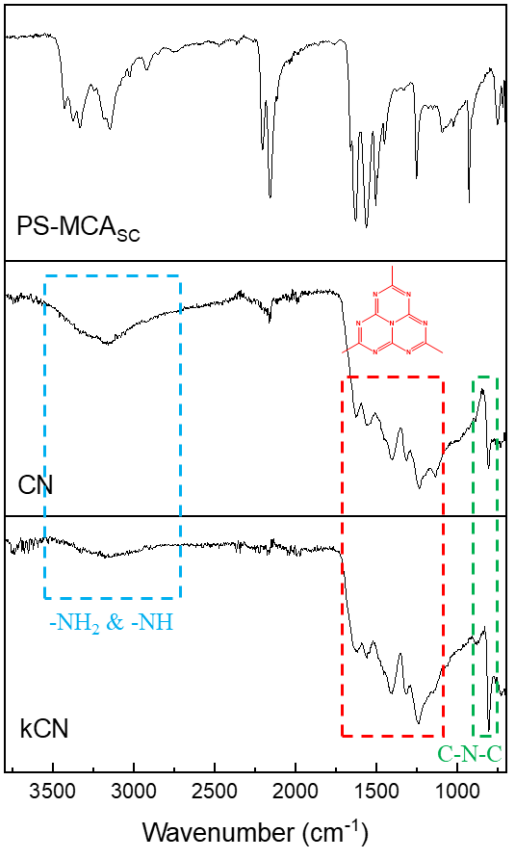

Figure 4-5. Infrared spectrum of carbon nitride obtained by different synthesis approaches. (Top) Untreated polystyrene with CN precursor film, (center) CN film, (bottom) kCN film.

4.2.2. Double-layer structure of photoanode

SEM images clearly show a double-layer structure of kCN (**Figure 4-6**). The microtubes of the porous top layer, originating from the film in the pretreatment step, increase the surface area of the kCN electrodes, while the second (bottom) layer, formed by the precursor vapor during CVD, is more condensed. In the sealed crucible, the high vapor pressure can easily penetrate the carbon skeleton and condense on the surface of the conductive substrate. This layer highly improves the affinity between the top layer and the substrate, influencing the charge transport ability inside the electrodes. The total thickness of the kCN film is around 1.8 µm, as shown by cross-section SEM (Fig. 2b). After scratching off the top porous layer, the second layer is observed as a transparent yellowish film with a thickness of around 100 nm. Therefore,

the thickness of the kCN film is mainly governed by the top layer. Thicker films can be obtained with higher polymer matrix concentrations, as observed in vertical scanning interferometry (VSI). Interestingly, the thickness of final films is slightly higher than that of the films after pretreatment, indicating the carbonization of polymer matrix into a porous carbon skeleton during the CVD process. Moreover, bandgaps are calculated to be 1.65 eV for the top layer and 2.71 eV for the bottom layer by the transformed Kubelka–Munk function. Based on Mott-Schottky (MS) plots, which give information on the flat band potential of semiconductor materials, we estimated the conduction band edges of the layers to be -0.77 V vs. RHE and -0.96 V vs. RHE for the top and bottom layer respectively. The narrow bandgap of the top layer can harvest a large portion of the solar spectrum. The valence band energy of the two layers differs significantly, resulting in the directed flow of photogenerated holes into the top layer. These holes can further contribute to the anode oxidation reaction.

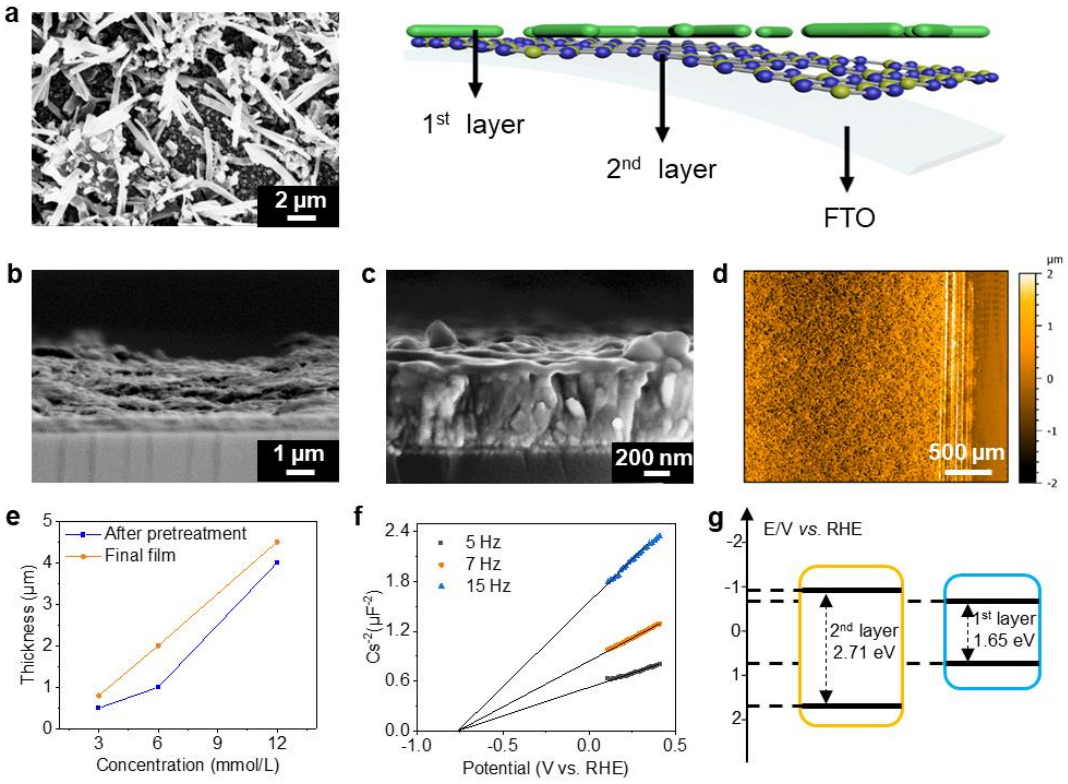

Figure 4-6. Layer structure of photoanode. (a) SEM image of kCN and schematic of the layer structure. Cross-section SEM image of kCN electrode (b) before and (c) after removal of the top layer. (d) Vertical scanning interferometry (VSI) measurement of the film after pretreatment. (e) Relationship between final kCN film thickness and film thickness after pretreatment depending on the concentration of polymer matrix. (f) Mott-Schottky plots of kCN. (g) Band structure of the two kCN layers.

4.2.3. Parameter scanning for optimized photoanodes

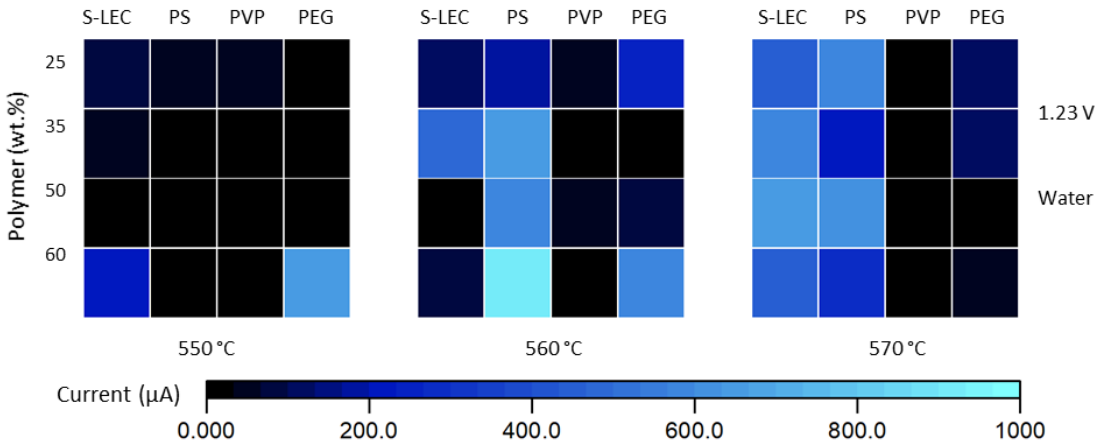

Figure 4-7. Parameter scanning for optimized photoanodes. Photocurrent density of kCN electrodes under different conditions (polymer type, polymer concentration, temperature, electrolyte, and applied bias).

The current densities of kCN electrodes under different conditions are shown in **Figure 4-7**. Four polymer matrixes were investigated: polystyrene acrylic copolymer (S-LEC), polystyrene (PS), polyvinylpyrrolidone ,(PVP) and polyethylene glycol (PEG). Both PS and S-LEC show extraordinary performance at higher synthesis temperatures (560-570 °C), while PEG requires relatively lower temperatures (550-560 °C). In the case of PVP, the electrodes are burnt/carbonated, therefore, it is not a suitable matrix for this synthesis method. In the aqueous electrolyte, photoanodes prepared with 60 % w/w PS at 560 °C give the highest current density of 975 µA cm^{-2}, which were used for further characterizations. The main strategy to improve the performance of CN electrodes is to build heterojunctions with metal oxides (**Figure 4-2**). However, kCN photoelectrodes exhibit much higher PEC properties than most reported CN-based electrodes, without the introduction of metal.

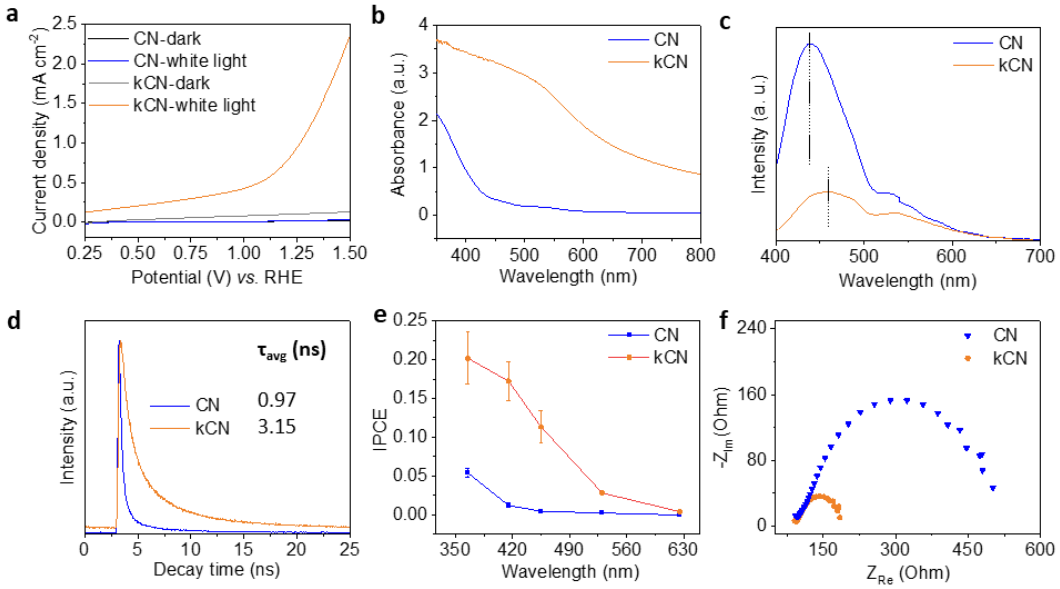

Figure 4-8. The PEC performance of optimized photoanodes. (a) Linear sweep voltammetry (LSV) curves of kCN and CN electrodes in 0.1 M Na_2SO_4 with and without light. (b) UV-visible absorption spectra. (c) Steady-state photoluminescence (PL) emission spectra. (d) Time-resolved transient PL decay spectra at 530 nm. (e) Incident photon-to-electron conversion efficiency (IPCE) plots. (f) Electrochemical impedance spectroscopy (EIS) Nyquist plots of electrodes in the dark.

Linear sweep voltammetry of the electrodes (**Figure 4-8a**) shows an about 100 times higher current density and reduced oxidation potential under white light irradiation in the kCN. A redshift up to 800 nm is observed in the UV-vis spectrum (**Figure 4-8b**), indicating that dopant and defect-related midgap states (MS) are generated in the forbidden gap of the normal CN. The calculated incident photon-to-current conversion efficiency (IPCE) of kCN electrodes at different illumination wavelengths (**Figure 4-8e**) shows a direct correlation with light absorption. A high IPCE value of 20.2 % is achieved at 365 nm, and a photoresponse can be detected up to 625 nm. Additionally, significant photoluminescence (PL) quenching occurs on the kCN electrodes in the steady-state PL emission spectra (**Figure 4-8c**), implying a strongly inhibited recombination of photogenerated electron-hole pairs. The redshift of the main PL peak in kCN indicates charge migration through the interface of the double-layer structure. The time-resolved transient PL decay spectra (**Figure 4-8d**) further prove that kCN has a longer average lifetime (τ_{avg}) of charge carriers with respect to the CN electrodes. The kCN electrodes show a smaller semicircle compared to CN electrodes (**Figure 4-8f**), indicating a much higher charge mobility and prolonged electron lifetime for kCN electrodes.

4.2.4. Performance of photoanodes in non-aqueous electrolytes

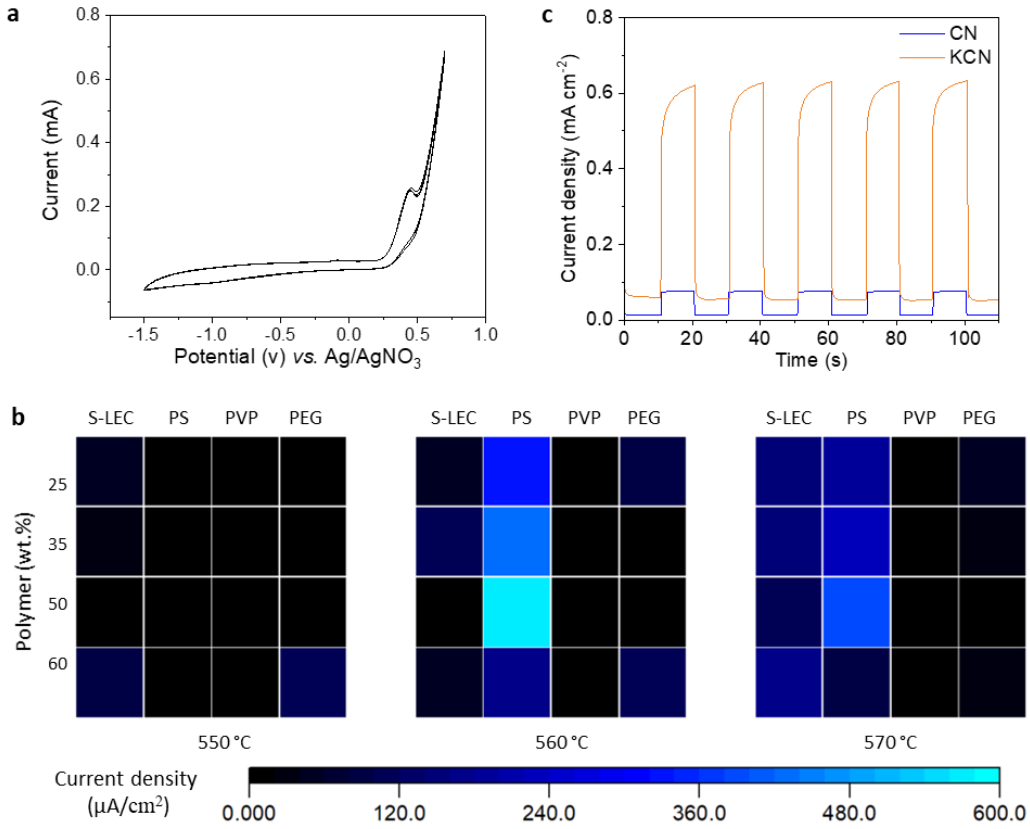

Figure 4-9. Performance of photoanodes in non-aqueous electrolytes. (a) Cyclic voltammogram of THIQ with platinum mesh as working electrode. (b) Current density of kCN electrodes under different synthesis conditions (polymer type, polymer concentration, and temperature) at +0.3 V vs. $Ag/AgNO_3$. (c) Transient photocurrent response of kCN and CN electrodes at +0.3 V vs. $Ag/AgNO_3$. All experiments were performed using 0.1 M $LiClO_4$ in methanol.

The extraordinarily high PEC properties enable the use of kCN photoanodes for organic transformations. As one of the most commonly exploited photocatalytic transformations, the oxidation of *N*-aryltetrahydroisoquinolines (THIQ) is an ideal model reaction to assess the performance of kCN photoelectrodes. The oxidation potential of THIQ begins at around +0.3 V vs. $Ag/AgNO_3$ electrode, according to cyclic voltammetry (**Figure 4-9a**). To optimize the electrodes for organic solvents, photocurrent densities of kCN electrodes were measured in methanol under the oxidation potential of THIQ (**Figure 4-9b**). Photoanodes generated with 50 % w/w PS at 560 °C give the highest current densities of 578 $\mu A/cm^2$, which were selected for the subsequent organic transformations. Its transient photocurrent under interval light irradiation shows a fast light response and stable current density (**Figure 4-9c**).

4.2.5. Optimization of reaction conditions and scope of the substrates

Table 4-1. Optimization of reaction conditions for the photoelectrocatalytic C–H functionalization

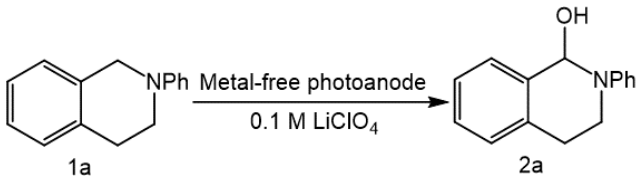

1a 2a

Entry	Anode	Applied bias[a]	Reaction time	Light	Solvent	Yield[b]
1	kCN	0.3 V	5 h	White light	ACN	86%
2	kCN	0.3 V	5 h	White light	Acetone	86%
3	kCN	0.3 V	5 h	White light	DMSO	100%
4	kCN	0.3 V	5 h	White light	MeOH	100%
5	kCN	0.3 V	2 h	White light	MeOH	100%
6	Pt mesh	0.61 V	2 h	No light	MeOH	19%
7	kCN	No bias	2 h	White light	MeOH	0

[a]Appiled bias vs. $Ag/AgNO_3$ electrode. [b]Yield is determined by NMR spectrum with CH_2Br_2 as the internal standard.

Based on the results from **Figure 4-9a**, the potential was set to 0.3 V vs. $Ag/AgNO_3$, resulting in a photocurrent of about 550 – 600 µA cm^{-2} using 0.1 M $LiClO_4$ in methanol. The reaction time was initially set to 5 h and various organic solvents were tested (**Table 4-1**, entry 1-4). Crude products were analyzed using NMR without further purification. The yields were calculated using CH_2Br_2 as an internal standard. Quantitative conversion of the starting material **1a** to the desired product **2a** was achieved within 2 h in methanol (**Table 4-1**, entry 5). For the control experiment, we chose the commonly used Pt mesh electrode as the anode (**Table 4-1**, entry 6). Since the Pt electrode is unable to respond to light irradiation, a potential of 0.61 V vs. $Ag/AgNO_3$ is necessary to reach the same current density. The yield only reached 19 % after 2 h, suggesting that the presence of light irradiation can not only reduce the input of electricity, but unambiguously points out that the photogenerated holes with higher oxidation potential enable electron transfer from THIQ. Another control experiment in the absence of applied bias was performed (**Table 4-1**, entry 7). In this situation, the kCN electrode can only function as a photocatalyst and no product was detected after 2 h reaction time. The PEC approach offers a highly efficient and environment-friendly way for the oxidation of THIQ. Therefore, we can conclude that this metal-free kCN photoanode can be applied for organic transformations. To show the applicability of the photoelectrocatalytic C–H functionalization approach we

explored a scope of substrates (**Table 4-2**) with previously optimized conditions (**Table 4-1**, entry 5). First, monosubstituted THIQ substrates were tested and quantitative conversion to the desired products **2b** and **2c** was observed. Multisubstituted THIQ were also suitable substrates (**2d**-**2f**), even though the yield slightly dropped in some cases (**2e**, **2f**), which might be caused by the formation of over-oxidation side products. In addition, THIQ with an electron-withdrawing group was oxidized to compound **2g** in good yield under the PEC conditions.

Table 4-2. Scope of N-aryltetrahydroisoquinoline derivatives for the photoelectrocatalytic C–H functionalization

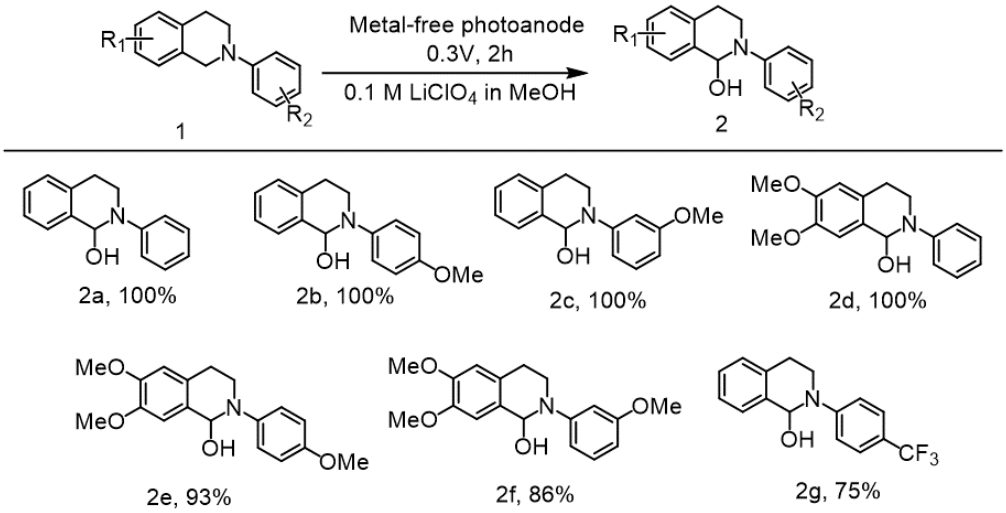

4.3. Conclusion

In conclusion, we have developed a facile method based on kinetic polymer reactors for the synthesis of kCN photoanodes, which show extraordinary PEC performance. This results from the double-layer structure of the kCN material: the porous top layer increases the interfacial area with electrolyte and the thin bottom layer improves the affinity between the films and the substrate. The dopant and defect-related midgap states (MS) in the forbidden band of the normal CN contribute to the efficient charge migration and separation, resulting in long charge lifetimes. Then, we show that metal-free photoanodes can be applied for C-H functionalization. A quantitative yield for the oxidation of THIQ can be reached without redox mediators, which is not achievable for commercially available platinum mesh electrodes, even under higher applied potential. This work opens a new avenue for cost-efficient and environmentally friendly metal-free photoanodes in organic synthesis.

5. Conclusion and outlook

This thesis significantly advances the polymer-assisted laser-induced forward transfer (polyLIFT) process in terms of both the performance of the technology and its applications. Furthermore, a new technology, called laser-driven transfer synthesis (LTRAS), derived from the polyLIFT principle, has been introduced. LTRAS not only achieves precise deposition of molecules as the standard polyLIFT method, but also enables *in-situ* synthesis of new materials with controllable morphologies.

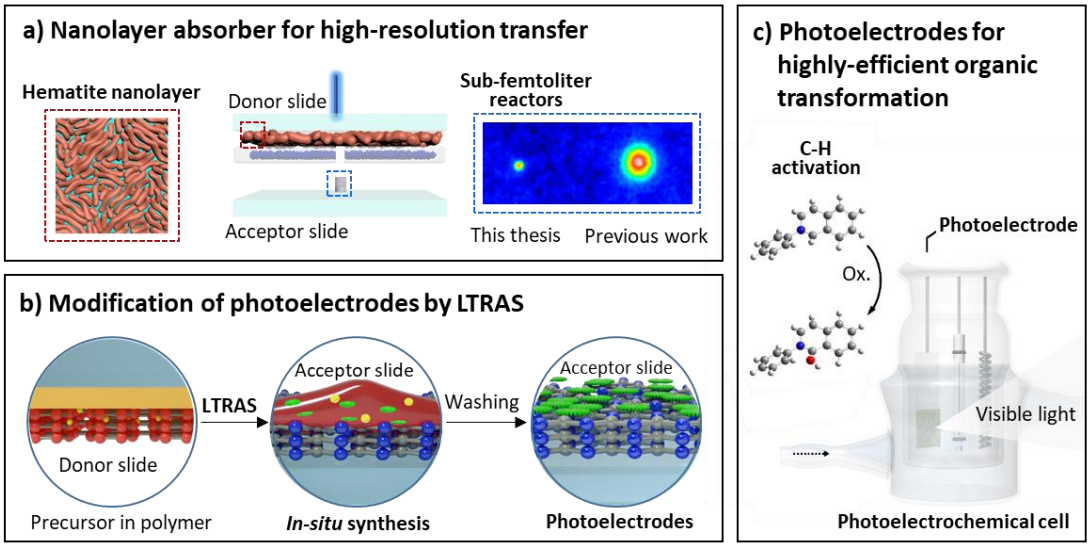

Figure 5-1. Summary of the thesis. a) Nanolayer laser absorber for polyLIFT (polymer assisted laser-induced forward transfer) process with five times higher patterning resolution (Chapter 2). b) *In-situ* synthesis of transition metal oxides by laser-driven transfer synthesis (LTRAS) for the modification of photoelectrodes (Chapter 3). c) Photoelectrodes for highly efficient organic transformations (Chapter 4).

In detail, we proposed a robust hematite (α-Fe_2O_3) nanolayer as the absorber for high-resolution polyLIFT to perform transfers down to the sub-femtoliter regime (**Figure 5-1a**). This is comparable with the resolution of atomic force microscopy-assisted microfluidic lithography (0.5 ± 0.2 fL *vs*. 42.7 ± 2.3 fL[27]), which is much more expensive and time-consuming. The nanolayer is wettable by both aqueous and organic solvents, significantly increasing the scope of polymers for the polyLIFT process. The highly improved transfer properties open up the possibility for new applications. The functionalization of photoelectrodes is one of these new applications. To achieve this, a new variant of the polyLIFT method, laser-driven transfer synthesis (LTRAS), has been introduced (**Figure 5-1b**). We showed that our continuous wave laser process can not only transfer, but also simultaneously drive a chemical reaction, to generate

precisely controlled transition metal oxide crystals on the surface of different substrates (*e.g.*, carbon nitride). The reaction can be completed within milliseconds and obtained composite films can be flexibly tuned with different particle shapes and sizes by the laser process. Due to the formation of heterojunctions (*i.e.*, a junction of two different semiconductors), the electrodes modified by the LTRAS process exhibit up to nine times higher photocurrents than the pristine electrodes. Therefore, LTRAS provides an efficient strategy for the preparation of high-performance photoelectrodes, which are actually the key component of photoelectrochemical (PEC) cells (**Figure 5-1c**). PEC reactions are an environmentally benign and sustainable pathway to synthesize value-added organic compounds by direct usage of solar energy. After optimization, we showed that carbon nitride-based photoelectrodes can be successfully applied for PEC C-H activation, which used to be a field dominated by metal-based photoelectrodes.

The ultimate purpose of this thesis was to establish the fundamental principles that guide laser-based material transfer and synthesis. For future work, several aspects can be envisioned:

1) The introduction of hematite donors highly improved the transfer quality and molecule/synthesis scope, however, the transfer mechanism of this new donor is not clear yet. A hypothesis suggests that the hematite absorber layer reaches much higher temperatures than the standard polyimide layer. More evidence for this should be provided in the future. Moreover, preliminary work shows that hematite donors can *in-situ* generate quantum dots in polymer reactors. The fluorescence signal may indicate the reached temperatures during the transfer process.
2) Even though we have shown that metal-free carbon nitride-based photoelectrodes can be successfully applied for PEC reactions in Chapter 4, the reactions performed are relatively simple. For the next stage, complex C-C coupling reactions should be tried, which might reveal more benefits of the PEC approach. Since these reactions have higher requirements for both the photocurrent and stability of photoelectrodes, further optimization of the electrodes is necessary. Therefore, an advanced LTRAS method will be expected to give a wider scope of semiconductor materials.
3) Due to the high transfer resolution achieved by hematite donors, the polyLIFT method becomes a promising approach for rapid nanomole-scale reaction screening. In combination with high-throughput analytics such as liquid chromatography–mass spectrometry (LC-MS), hundreds of reactions with thousands of data points can be performed in a matter of days or even hours. These newly designed experimental approach may drastically accelerate the

discovery of catalysts or pharmaceutical agents and minimize the cost/time spent on ultimately non-optimal analogs.

6. Experimental section

6.1. General materials and methods

Chemicals and solvents were purchased from commercial suppliers and used as received. For the characterization of materials, scanning electron microscopy (SEM) studies were carried out using a Zeiss LEO 1550 microscope equipped with a field emission gun and with an Oxford Instruments X-MAX SDD X-ray energy-dispersive detector (detection area is 80 mm²). X-ray powder diffraction (XRD) patterns were collected with an X-ray powder diffractometer Bruker D8 using Cu Kα radiation (λ = 0.15418 nm). Optical absorbance spectra of donors were measured with a PG Instruments TG70+ UV/Vis Spectrometer. For transmission electron microscopy (TEM) observations, the analyses were performed using a double Cs corrected JEOL JEM-ARM200F (S)TEM operated at 80kV and equipped with a cold-field emission gun and a high-angle silicon drift Energy Dispersive X-ray (EDX) detector (solid angle up to 0.98 steradians with a detection area of 100 mm^2). Selected area electron diffraction patterns were recorded at cryogenic temperature using an Elsa cryo holder (Gatan, the U.S.A). Contact angles at the three-phase contact line were determined from side view images, taken with a custom side view setup. Spot volumes and film thickness measurements are based on a smartWLI compact (Gesellschaft für Bild- und Signalverarbeitung (GBS) mbH, Illmenau, Germany) with low magnification (5× Nikon CF IC Epi Plan DI—Mirau). Further data analysis was performed in MountainsMap 8.0 with threshold detection method and step method, respectively.

6.2. General procedure for LIFT

6.2.1. Laser setup

We use a 200 mW TOPTICA iBeam smart 488-S laser with a wavelength of 488 nm (TOPTICA Photonics AG, Germany) that can be flexibly tuned in power and pulse duration. The laser is passed through a 1:10 beam expander, before entering a Racoon 11 laser scanning system (ARGES GmbH, Germany), which is equipped with an f-Theta lens (S4LFT5110/322, Sill Optics GmbH, Germany), as shown for LIFT-based array generation. This setup allows us to scan the laser focus with a defined speed in a plane of 66 mm x 66 mm, enabling reproducible irradiation of a surface at various positions within the lasing area, with a $1/e^2$ laser spot diameter of 18 µm.

A second laser setup is equipped with a 405 nm laser with 100 mW power. Briefly, a commercial laser engraving system was upgraded with a microcontroller, to have full control over pattern, laser power, and laser pulse duration.[28] The laser is attached to

two mechanical axes, which move the laser in a plane above the sample surface. The $1/e^2$ laser spot diameter is 42 µm.

6.2.2. Preparation of donor slides

For hematite donors, 125 mg of PVA (polyvinyl alcohol, av. *Mw*=9000~10000, Sigma) and 125 mg of $Fe(NO_3)_3 \cdot 9H_2O$ (98 %, Acros) were dissolved in 250 µl of ddH_2O. 250 mg of PEG (Polyethylene glycol, av. *M*w ≈20 000, Sigma) and 250 mg of $Fe(NO_3)_3 \cdot 9H_2O$ were dissolved in 250 µl of methanol. The two solutions were mixed by stirring for 20 min and sonicated for another 20 min. The ink preparation is a critical step for the hematite nanolayer synthesis. To remove potential residual bubbles from the solution, longer stirring and sonication times may be required. Then, the solution was spin coated onto a clean glass slide at 70 rps and the slide was placed in an oven which was set to keep 500 °C for 3 h. After cooling down, the final hematite slide was obtained.

Polyimide donors were prepared by simply laminating commercially available self-adhesive 25 µm thin Kapton film (HN 100 type, Dupont, USA; CMC Klebetechnik, Germany) onto glass slides.

6.2.3. LIFT patterning process

For the typical polymer solution, 30 mg PS (polystyrene, av. *Mw* = 35 000, Sigma) were dissolved in 500 µL of DCM. We spin-coated the solution on donor slides at 70 rps to get a homogeneous material layer. After cleaning the backside of the donor slide, we placed it on the top of a clean glass which served as the acceptor and transferred the material with the respective laser system. The transferred materials were either characterized by fluorescent images with a Genepix 4000B scanner (Molecular Devices, USA) or vertical scanning interferometry with a smartWLI compact (Gesellschaft für Bild- und Signalverarbeitung (GBS) mbH, Illmenau, Germany).

6.3. LTRAS for the modification of photoelectrodes

6.3.1. Preparation of TMO/CN electrodes

Acceptor slide: A clean fluorine-doped tin oxide (FTO) coated glass (6 cm x 6 cm, 7 Ω/sq, Merck) covered a 29.5 mL rectangular alumina crucible with 5 g melamine (99 %, Alfa Aesar). We placed the crucible in a furnace (CMF-1200, Carbolite Gero, UK), set to 550 °C, incrementing by 1.5 °C/min and kept at 550 °C for 3 h under nitrogen. The as-prepared slides were cut into small pieces (1 x 1.5 cm) and used as CN electrodes.

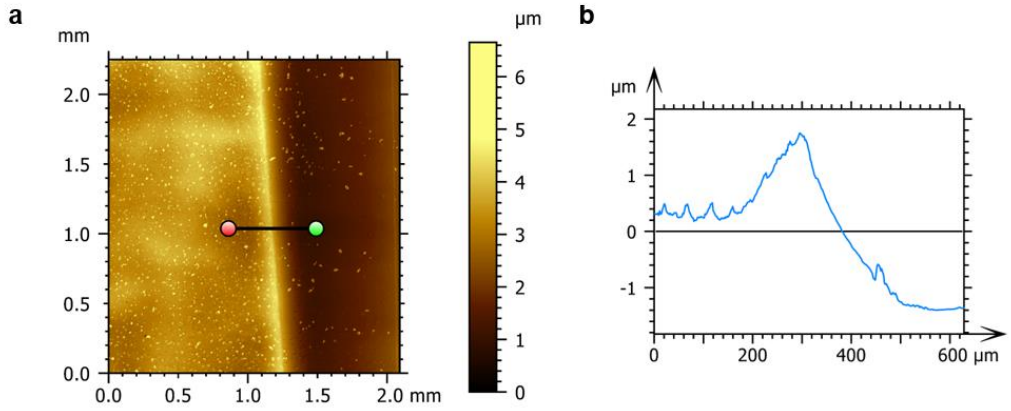

Figure 6-1. (a) Vertical scanning interferometry (VSI) measurement of donor slide and (b) thickness profile.

Donor slide: 10, 20, or 30 mg $Cu(NO_3)_2 \cdot xH_2O$ (99 %, Acros) and 30 mg copolymer (S-LEC PLT 7552, Sekisui Chemical GmbH, Germany) were dissolved in the mixture of 50 µL N,N-dimethylformamide, 100 µL acetonitrile, and 350 µL dichloromethane. All solvents were used as obtained from Sigma-Aldrich. We spin-coated the solution on polyimide film (Kapton HN 100 type, Dupont, USA) covered glasses at 80 rps. The thickness of the obtained polymer film measured around 1.5 µm in vertical scanning interferometry (**Figure 6-1**). The obtained slides are the so called 'donor slides'. Due to the difference of solubility, 10 mg $Ni(NO_3)_2.6H_2O$ (99 %, Roth) and 20 mg $Co(NO_3)_2.6H_2O$ (98%, Sigma-Aldrich) precursors were used in the preparation of the donor slides for the NiO and CoO nanostructures, respectively.

6.3.2. Photoelectrochemical measurements

6.3.2.1. Measurements and calculations

Transient photocurrent density, linear sweep voltammograms, and chronopotentiometry were measured by a three-electrode potentiostat (BioLogic MPG2). A Pt electrode (ALS Co., Ltd, Japan), a Ag/AgCl in sat. KCl filling solution (ALS Co., Ltd, Japan), and 0.1 M NaOH solution are used as the counter electrode, reference electrode, and electrolyte respectively. The photocurrent with reference to reversible hydrogen electrode (RHE) is calculated with the following formula:

$$E_{(RHE)} = E_{Ag/AgCl} + 0.059\, pH + E^0_{Ag/AgCl}$$

where $E_{Ag/AgCl}$ is the applied working potential, $E^0_{Ag/AgCl}$ = 0.1976 V at 25 °C.

Faradaic efficiency (FE) is measured at 1.23 V vs. RHE and calculated by the following equation:

$$FE(\%) = \frac{m \cdot n \cdot \mathrm{F}}{I \cdot t} \times 100$$

where *m* is the amount of oxygen (mol), *n* is the number of reaction electrons, F is the Faraday constant, *I* is the photocurrent (A), and *t* is the reaction time (s).

Incident photon-to-current conversion efficiency (IPCE) is calculated by the following formula:

$$IPCE(\%) = \frac{J_{Ph}\,(A/cm^2) \times 1240\ (V \cdot nm)}{\lambda(nm) \times J_{Light}(W/cm^2)}$$

where J_{Ph} is the photocurrent density, λ the wavelength, and J_{Light} is the intensity of incident light. A series of fiber-coupled LEDs (SMA, ThorLabs) with wavelengths of 415 nm, 455 nm, 530 nm, 625 nm, and 850 nm were connected to the LED Driver (DC2200, ThorLabs) and used as light sources for the IPCE measurements. For each wavelength, we studied the dependence of current density versus intensity of the incident light (5 data points). The current density depends linearly on the intensity of the incident light. The slope of linear fitting corresponds to the ratio between J_{Ph} and J_{Light}.

The flat band potential was calculated with the Mott-Schottky equation (15 Hz, without light):

$$\frac{1}{C^2} = \frac{2}{N_D e \varepsilon \varepsilon_0} \cdot \left[\left(V_S - V_{fb}\right) - \frac{k_B T}{e}\right]$$

where *C* is the space-charge capacitance, V_S is the applied potential, V_{fb} is the flat band potential, N_D is the electron carrier density, ε is the relative permittivity of the semiconductor, ε_0 is the permittivity of the vacuum, *e* is the elementary charge, and k_B is the Boltzmann constant.

6.3.2.2. Glucose detection by amperometry

The response of the pristine CN and the composite CuO_{F1}/CN electrodes to glucose was evaluated using amperometry by successively adding small amounts of concentrated glucose solution. In detail, the phototelectrochemicial performance was assessed using a three-electrode cell. Pt electrode, Ag/AgCl in saturated KCl, and 0.1 M NaOH solution were used as counter electrode, reference electrode, and electrolyte respectively. We added 100 µl of glucose solution into 20 ml of 0.1 M NaOH electrolyte in 30 s intervals. The concentrations of glucose solution used in this experiment were 10 mM, 10 mM, 20 mM, 20 mM, and 40 mM, respectively. In the electrolyte, we obtained glucose concentrations in the range from 0.05 to 0.5 mM. The measurements were performed at 0.1 V *vs.* Ag/AgCl under white light (300 mW/cm^2) or blue light (100 mW/cm^2).

6.3.3. Preparation of the control electrodes

6.3.3.1. Cu-based CN electrodes from photodeposition

270 mg of $Cu(NO_3)_2 \cdot xH_2O$ (99 %, Acros) were dissolved in 3 ml ddH_2O in a petri dish (⌀ 25 mm), and a piece of FTO glass (7 Ω/sq, Merck) with a CN layer was immersed in this precursor solution. Then, the petri dish was placed under a laser irradiation system (1.9 W, 450 nm) and irradiated to create a 10 x 10 pattern (full power, 100 – 450 ms). Moreover, a piece of CN substrate was immersed in 0.1 M $Cu(NO_3)_2 \cdot xH_2O$ solution under UV light for several hours (1 h, 2 h, or 4 h). The photoelectrochemical performance was measured in a three-electrode cell. Pt electrode, Ag/AgCl in saturated KCl, and 0.1 M NaOH solution were used as the counter electrode, reference electrode, and electrolyte respectively.

6.3.3.2. Cu-based CN electrodes from co-polymerization

0.1wt.%, 1wt.%, or 10wt.% $Cu(NO_3)_2 \cdot xH_2O$ (99 %, Acros) and 5 g melamine (99 %, Alfa Aesar) were added in 50 ml ddH_2O and stirred at 80 °C for 2 h. Afterwards, we removed the water by centrifugation (8000 rpm, 2 min). The obtained material was dried in an oven at 80 °C and labeled as “Cu-M”. We put the Cu-M into a crucible and calcined it in a furnace (570 °C, 3 h). Then, the powder was washed three times with ddH_2O to remove possible remaining precursor and intermediates with lower polymerization degree. According to the amount of Cu precursor, the final powder is labeled as $Cu_{0.1}$-CN, Cu_1-CN, or Cu_{10}-CN. In the next step, following the typical protocol for the preparation of photoelectrodes from CN powder, we deposited these pre-synthesized powders on the electrodes. Briefly, 2 mg of $Cu_{0.1}$-CN, Cu_1-CN, or Cu_{10}-CN and 20 µl Nafion solution (5 wt. %, Aldrich) were mixed with 200 µl of ddH_2O. After ultrasound treatment for 1 h, we deposited the suspension on the FTO substrate by doctor blading. All electrodes were prepared with a 1 cm x 1 cm area of the light-responsive Cu_x-CN material. The photoelectrochemical performance was measured in a three-electrode cell. Pt electrode, Ag/AgCl in saturated KCl, and 0.1 M NaOH solution were used as the counter electrode, reference electrode, and electrolyte respectively.

6.4. Organic transformation

6.4.1. polyLIFT$_h$-based amino acid coupling

Acceptor slide: We used a PEGMA-*co*-MMA Fmoc-β-alanine (PEPperPRINT GmbH, Germany) functionalized surface as the acceptor slide. The slide was swelled for 20 min in DMF and Fmoc-deprotected for another 20 min by 20% (v/v) piperidine in DMF, followed by washing. The standard washing procedure was performed as described:

the slide was immersed three times in DMF for 10 min, one time in methanol for 2 min, one time in DCM for 1 min and finally dried in a jet of compressed air.

Donor slide: 30 mg PS (polystyrene, av. *Mw*=35 000, Sigma) and 3 mg pentafluorophenyl ester (OPfp)-activated glycine were dissolved in 500 µL of DCM. We spin-coated the solution on donor slides at 70 rps to get a homogeneous material layer.

Coupling and staining: After the patterning of an acceptor slide, we initiated the coupling reaction by heating the acceptor slide to 95 °C for 10 min under nitrogen atmosphere. Afterwards, the unreacted amino groups on the acceptor were capped twice with capping reagents (mix of 10% acetic anhydride, 20% DIPEA, 70% DMF (v/v/v)) for 30 min. After another deprotection step by piperidine solution and washing, we incubated the acceptor with 0.1 µg/mL DyLight™ 633 NHS in 10 mL PBS-T solution for 1 h. After another short washing step, the donor slide was scanned at a wavelength of 635 nm (laser power: 33%, resolution: 5 µm, photo multiplier (PMT): 600).

6.4.2. polyLIFT$_h$-based click chemistry

Acceptor slide: We used a PEGMA-*co*-MMA Fmoc-β-alanine (PEPperPRINT GmbH, Germany) functionalized surface as the acceptor slide. Two slides were swelled for 20 min in DMF and deprotected for another 20 min by 20% (v/v) piperidine in DMF, followed by washing. The standard washing procedure was performed as described: the slides were immersed three times in DMF for 10 min, one time in methanol for 2 min, one time in DCM for 1 min and finally dried by compressed air. One slide without further functionalization was used as a control to confirm that no non-covalent binding occurred. For another slide, 11 µL azidoacetic acid was dissolved in 166 µL DMF (peptide synthesis grade), following with the addition of 23 µL *N*,*N*'-diisopropylcarbodiimide and 27.3 mg pentafluorophenol. The freshly prepared solution was poured between the acceptor slide and a clean glass slide, then shaking it overnight in the dark. After the standard washing procedure, the acceptor slide was dried in a jet of compressed air.

Donor slide: 5.3 mg $CuSO_4$ and 10.0 mg sodium ascorbate were added to 160 µL water in separate tubes. After shaking for 2 min, the two solutions were mixed, and then 320 µL of turbid solution with orange color was obtained. The precipitate was centrifuged and the remaining solution was passed through a syringe filter (0.45 µm, polypropylene), followed by the addition of 60 mg PVA (av. *Mw*=9000~10000). 5 mg Alk-DQ was dissolved in 200 µl DMSO and added into the filtered solution. The as-prepared solution was spin-coated on the hematite donor at 50 rps.

6.4.3. polyLIFT$_h$-based *in-situ* oxidation

6,7-dimethoxy-2-(3-methoxyphenyl)-1,2,3,4-tetrahydroisoquinoline (TM-THIQ) was synthesized according to the literature.[29] 30 mg PS (polystyrene, av. *Mw* = 35 000, Sigma), 3 mg TM-THIQ and 100 µl CBr_3Cl were dissolved in 400 µL of DCM. We spin-coated the solution on a donor slide with 70 rps to get a homogeneous material layer. This freshly prepared donor slide was used for laser transfer. After patterning on a clean glass slide, we scanned it at a wavelength of 532 nm (laser power: 33%, resolution: 5 µm, PMT: 600). Then, the patterns were washed with methanol (HPLC grade) and moved into a glass vial for liquid chromatography–mass spectrometry (LC–MS).

The Density Functional Theory (DFT) calculations were performed with the Gaussian 09 package. Structural optimizations and frequency calculations were performed with the B3LYP hybrid functional description with D3 dispersion correction and Becke-Johnson (BJ) damping at the basis set level of 6-31G*.

6.4.4. Photoelectrochemical C-H activation reaction

To prepare the reaction solution for the PEC cell with the metal-free carbon nitride electrodes, 50 µmol of substrate and 0.5 mmol $LiClO_4$ were dissolved in 5 ml solvent (typically MeOH). A potential at 0.3 V vs. Ag/AgNO3 reference electrode is applied in the three-electrode potentiostat. The reaction is performed under white light irradiation for several hours (typically 2 h), with the running of cooling water at 25 °C.

7. References

1. J. Bohandy, B. F. K., and F. J. Adrian Metal deposition from a supported metal film using an excimer laser. *J. Appl. Phys.* **1986,** *60*.

2. Patrascioiu, A.; Fernández-Pradas, J. M.; Palla-Papavlu, A.; Morenza, J. L.; Serra, P., Laser-generated liquid microjets: correlation between bubble dynamics and liquid ejection. *Microfluid. Nanofluid.* **2014,** *16* (1), 55-63.

3. Palla Papavlu, A.; Mattle, T.; Temmel, S.; Lehmann, U.; Hintennach, A.; Grisel, A.; Wokaun, A.; Lippert, T., Highly sensitive SnO2 sensor via reactive laser-induced transfer. *Sci. Rep.* **2016,** *6* (1), 25144.

4. Papazoglou, S.; Zergioti, I., Laser Induced Forward Transfer (LIFT) of nano-micro patterns for sensor applications. *Microelectron. Eng.* **2017,** *182*, 25-34.

5. Serra, P.; Piqué, A., Laser-Induced Forward Transfer: Fundamentals and Applications. *Adv. Mater. Technol.* **2019,** *4* (1), 1800099.

6. Nagl, S.; Schaeferling, M.; Wolfbeis, O. S., Fluorescence Analysis in Microarray Technology. *Microchim. Acta* **2005,** *151* (1), 1-21.

7. Würth, C.; Grabolle, M.; Pauli, J.; Spieles, M.; Resch-Genger, U., Relative and absolute determination of fluorescence quantum yields of transparent samples. *Nat. Protoc.* **2013,** *8* (8), 1535-1550.

8. Resch-Genger, U.; Grabolle, M.; Cavaliere-Jaricot, S.; Nitschke, R.; Nann, T., Quantum dots versus organic dyes as fluorescent labels. *Nat. Methods* **2008,** *5* (9), 763-775.

9. Resch-Genger, U.; Hoffmann, K.; Nietfeld, W.; Engel, A.; Neukammer, J.; Nitschke, R.; Ebert, B.; Macdonald, R., How to Improve Quality Assurance in Fluorometry: Fluorescence-Inherent Sources of Error and Suited Fluorescence Standards. *J. Fluoresc.* **2005,** *15* (3), 337-362.

10. RamalloGuevara, C.; Paulssen, D.; Popova, A. A.; Hopf, C.; Levkin, P. A., Fast Nanoliter-Scale Cell Assays Using Droplet Microarray–Mass Spectrometry Imaging. *Adv. Biol.* **2021,** *5* (3), 2000279.

11. Stewart, J. S.; Lippert, T.; Nagel, M.; Nüesch, F.; Wokaun, A., Red-green-blue polymer light-emitting diode pixels printed by optimized laser-induced forward transfer. *Appl. Phys. Lett.* **2012,** *100* (20), 203303.

12. Piqué, A.; Auyeung, R. C. Y.; Kim, H.; Charipar, N. A.; Mathews, S. A., Laser 3D micro-manufacturing. *J. Phys. D: Appl. Phys.* **2016,** *49* (22), 223001.

13. Kim, H.; Duocastella, M.; Charipar, K. M.; Auyeung, R. C. Y.; Piqué, A., Laser printing of conformal and multi-level 3D interconnects. *Appl. Phys. A* **2013,** *113* (1), 5-8.

14. Visser, C. W.; Pohl, R.; Sun, C.; Römer, G.-W.; Huis in ‘t Veld, B.; Lohse, D., Toward 3D Printing of Pure Metals by Laser-Induced Forward Transfer. *Adv. Mater.* **2015,** *27* (27), 4087-4092.

15. Arnold, C. B.; Wartena, R. C.; Swider-Lyons, K. E.; Pique, A., Direct-Write Planar Microultracapacitors by Laser Engineering. *J. Electrochem. Soc.* **2003,** *150* (5), A571.

16. Riggs, B. C.; Dias, A. D.; Schiele, N. R.; Cristescu, R.; Huang, Y.; Corr, D. T.; Chrisey, D. B., Matrix-assisted pulsed laser methods for biofabrication. *MRS Bull.* **2011,** *36* (12), 1043-1050.

17. Colina, M.; Serra, P.; Fernández-Pradas, J. M.; Sevilla, L.; Morenza, J. L., DNA deposition through laser induced forward transfer. *Biosens. Bioelectron.* **2005,** *20* (8), 1638-1642.

18. Loeffler, F. F.; Foertsch, T. C.; Popov, R.; Mattes, D. S.; Schlageter, M.; Sedlmayr, M.; Ridder, B.; Dang, F.-X.; von Bojničić-Kninski, C.; Weber, L. K.; Fischer, A.; Greifenstein, J.; Bykovskaya, V.; Buliev, I.; Bischoff, F. R.; Hahn, L.; Meier, M. A. R.; Bräse, S.; Powell, A. K.; Balaban, T. S.; Breitling, F.; Nesterov-Mueller, A., High-flexibility combinatorial peptide synthesis with laser-based transfer of monomers in solid matrix material. *Nat. Commun.* **2016,** *7* (1), 11844.

19. Ringeisen, B. R.; Wu, P. K.; Kim, H.; Piqué, A.; Auyeung, R. Y. C.; Young, H. D.; Chrisey, D. B.; Krizman, D. B., Picoliter-Scale Protein Microarrays by Laser Direct Write. *Biotechnol. Prog.* **2002,** *18* (5), 1126-1129.

20. Serra, P.; Fernández-Pradas, J. M.; Berthet, F. X.; Colina, M.; Elvira, J.; Morenza, J. L., Laser direct writing of biomolecule microarrays. *Appl. Phys. A* **2004,** *79* (4), 949-952.

21. Duocastella, M.; Fernández-Pradas, J. M.; Domínguez, J.; Serra, P.; Morenza, J. L., Printing biological solutions through laser-induced forward transfer. *Appl. Phys. A* **2008,** *93* (4), 941-945.

22. Barron, J. A.; Young, H. D.; Dlott, D. D.; Darfler, M. M.; Krizman, D. B.; Ringeisen, B. R., Printing of protein microarrays via a capillary-free fluid jetting mechanism. *Proteomics* **2005,** *5* (16), 4138-4144.

23. Dinca, V.; Farsari, M.; Kafetzopoulos, D.; Popescu, A.; Dinescu, M.; Fotakis, C., Patterning parameters for biomolecules microarrays constructed with nanosecond and femtosecond UV lasers. *Thin Solid Films* **2008,** *516* (18), 6504-6511.

24. Papazoglou, S.; Tsouti, V.; Chatzandroulis, S.; Zergioti, I., Direct laser printing of graphene oxide for resistive chemosensors. *Opt. Laser Technol.* **2016,** *82*, 163-169.

25. Tsouti, V.; Boutopoulos, C.; Goustouridis, D.; Zergioti, I.; Normand, P.; Tsoukalas, D.; Chatzandroulis, S., A chemical sensor microarray realized by laser printing of polymers. *Sens. Actuators, B* **2010,** *150* (1), 148-153.

26. Di Pietrantonio, F.; Benetti, M.; Cannatà, D.; Verona, E.; Palla-Papavlu, A.; Dinca, V.; Dinescu, M.; Mattle, T.; Lippert, T., Volatile toxic compound detection by surface acoustic wave sensor array coated with chemoselective polymers deposited by laser induced forward transfer: Application to sarin. *Sens. Actuators, B* **2012,** *174*, 158-167.

27. Cannatà, D.; Benetti, M.; Di Pietrantonio, F.; Verona, E.; Palla-Papavlu, A.; Dinca, V.; Dinescu, M.; Lippert, T., Nerve agent simulant detection by solidly mounted resonators (SMRs) polymer coated using laser induced forward transfer (LIFT) technique. *Sens. Actuators, B* **2012,** *173*, 32-39.

28. Sackmann, E. K.; Fulton, A. L.; Beebe, D. J., The present and future role of microfluidics in biomedical research. *Nature* **2014,** *507* (7491), 181-189.

29. Dudukovic, N. A.; Fong, E. J.; Gemeda, H. B.; DeOtte, J. R.; Cerón, M. R.; Moran, B. D.; Davis, J. T.; Baker, S. E.; Duoss, E. B., Cellular fluidics. *Nature* **2021,** *595* (7865), 58-65.

30. Chen, P. C.; Liu, M. H.; Du, J. S. S.; Meckes, B.; Wang, S. Z.; Lin, H. X.; Dravid, V. P.; Wolverton, C.; Mirkin, C. A., Interface and heterostructure design in polyelemental nanoparticles. *Science* **2019,** *363* (6430), 959.

31. Chen, P. C.; Liu, X. L.; Hedrick, J. L.; Xie, Z.; Wang, S. Z.; Lin, Q. Y.; Hersam, M. C.; Dravid, V. P.; Mirkin, C. A., Polyelemental nanoparticle libraries. *Science* **2016,** *352* (6293), 1565-1569.

32. Jia, X.; Jiang, J.; Zou, S.; Han, L.; Zhu, H.; Zhang, Q.; Ma, Y.; Luo, P.; Wu, P.; Mayoral, A.; Han, X.; Cheng, J.; Che, S., Library Creation of Ultrasmall Multi-metallic Nanoparticles Confined in Mesoporous MFI Zeolites. *Angew. Chem., Int. Ed.* **2021,** *60* (26), 14571-14577.

33. Gupta, N.; Lin, B. F.; Campos, L. M.; Dimitriou, M. D.; Hikita, S. T.; Treat, N. D.; Tirrell, M. V.; Clegg, D. O.; Kramer, E. J.; Hawker, C. J., A versatile approach to high-throughput microarrays using thiol-ene chemistry. *Nat. Chem.* **2010,** *2* (2), 138-145.

34. Zhang, Y.; Minagawa, Y.; Kizoe, H.; Miyazaki, K.; Iino, R.; Ueno, H.; Tabata, K. V.; Shimane, Y.; Noji, H., Accurate high-throughput screening based on digital protein synthesis in a massively parallel femtoliter droplet array. *Sci. Adv.* **2019,** *5* (8), eaav8185.

35. Carbonell, C.; Stylianou, K. C.; Hernando, J.; Evangelio, E.; Barnett, S. A.; Nettikadan, S.; Imaz, I.; Maspoch, D., Femtolitre chemistry assisted by microfluidic pen lithography. *Nat. Commun.* **2013,** *4* (1), 2173.

36. Liu, X.; Carbonell, C.; Braunschweig, A. B., Towards scanning probe lithography-based 4D nanoprinting by advancing surface chemistry, nanopatterning strategies, and characterization protocols. *Chem. Soc. Rev.* **2016,** *45* (22), 6289-6310.

37. Garcia, R.; Knoll, A. W.; Riedo, E., Advanced scanning probe lithography. *Nat. Nanotechnol.* **2014,** *9* (8), 577-587.

38. Howell, S. T.; Grushina, A.; Holzner, F.; Brugger, J., Thermal scanning probe lithography—a review. *Microsyst. Nanoeng.* **2020,** *6* (1), 21.

39. Eickelmann, S.; Tsouka, A.; Heidepriem, J.; Paris, G.; Zhang, J.; Molinari, V.; Mende, M.; Loeffler, F. F., A Low-Cost Laser-Based Nano-3D Polymer Printer for Rapid Surface Patterning and Chemical Synthesis of Peptide and Glycan Microarrays. *Adv. Mater. Technol.* **2019,** *4* (11), 1900503.

40. Ryu Y.K., K. A. W., *Electrical Atomic Force Microscopy for Nanoelectronics*. 2019.

41. Zhang, J.; Zou, Y.; Eickelmann, S.; Njel, C.; Heil, T.; Ronneberger, S.; Strauss, V.; Seeberger, P. H.; Savateev, A.; Loeffler, F. F., Laser-driven growth of structurally defined transition metal oxide nanocrystals on carbon nitride photoelectrodes in milliseconds. *Nat. Commun.* **2021,** *12* (1), 3224.

42. Eickelmann, S.; Ronneberger, S.; Zhang, J.; Paris, G.; Loeffler, F. F., Alkanes as Intelligent Surface Thermometers: A Facile Approach to Characterize Short-Lived Temperature Gradients on the Micrometer Scale. *Adv. Mater. Interfaces* **2021,** *8* (3), 2001626.

43. Mende, M.; Tsouka, A.; Heidepriem, J.; Paris, G.; Mattes, D. S.; Eickelmann, S.; Bordoni, V.; Wawrzinek, R.; Fuchsberger, F. F.; Seeberger, P. H.; Rademacher, C.; Delbianco, M.; Mallagaray, A.; Loeffler, F. F., On-Chip Neo-Glycopeptide Synthesis for Multivalent Glycan Presentation. *Chem. - Eur. J.* **2020,** *26* (44), 9954-9963.

44. Paris, G.; Klinkusch, A.; Heidepriem, J.; Tsouka, A.; Zhang, J.; Mende, M.; Mattes, D. S.; Mager, D.; Riegler, H.; Eickelmann, S.; Loeffler, F. F., Laser-induced forward transfer of soft material nanolayers with millisecond pulses shows contact-based material deposition. *Appl. Surf. Sci.* **2020,** *508*, 144973.

45. Mathevula, L. E.; Noto, L. L.; Mothudi, B. M.; Chithambo, M.; Dhlamini, M. S., Structural and optical properties of sol-gel derived α-Fe2O3 nanoparticles. *Journal of Luminescence* **2017,** *192*, 879-887.

46. Sopeña, P.; Serra, P.; Fernández-Pradas, J. M., Transparent and conductive silver nanowires networks printed by laser-induced forward transfer. *Appl. Surf. Sci.* **2019,** *476*, 828-833.

47. Liu, Y.; Seeberger, P. H.; Merbouh, N.; Loeffler, F. F., Position Matters: Fluorescent Positional Isomers for Reversible Multichannel Encryption Devices. *Chem. - Eur. J.* **2021**, 10.1002/chem.202103441.

48. Lin, L.; Lin, Z.; Zhang, J.; Cai, X.; Lin, W.; Yu, Z.; Wang, X., Molecular-level insights on the reactive facet of carbon nitride single crystals photocatalysing overall water splitting. *Nat. Catal.* **2020**.

49. Ye, K. H.; Li, H. B.; Huang, D.; Xiao, S.; Qiu, W. T.; Li, M. Y.; Hu, Y. W.; Mai, W. J.; Ji, H. B.; Yang, S. H., Enhancing photoelectrochemical water splitting by combining work function tuning and heterojunction engineering. *Nat. Commun.* **2019,** *10*, 9.

50. Karjule, N.; Barrio, J.; Xing, L. D.; Volokh, M.; Shalom, M., Highly Efficient Polymeric Carbon Nitride Photoanode with Excellent Electron Diffusion Length and Hole Extraction Properties. *Nano Lett.* **2020,** *20* (6), 4618-4624.

51. Zhao, L.; Kuang, X.; Liu, Z.; Hou, Y.; Wang, Z.; Wei, Q.; Lee, J. Y.; Kang, B., Anchoring CuO Nanoparticles On C, N-Codoped G-C3N4 Nanosheets from Melamine-Entrapped MOF Gel for High-Efficiency Oxygen Evolution. *ChemNanoMat* **2019,** *5* (9), 1170-1175.

52. Wang, Y.; Wu, N. N.; Wang, Y.; Ma, H.; Zhang, J. X.; Xu, L. L.; Albolkany, M. K.; Liu, B., Graphite phase carbon nitride based membrane for selective permeation. *Nat. Commun.* **2019,** *10*, 8.

53. Mohamed, H. S. H.; Wu, L.; Li, C.-F.; Hu, Z.-Y.; Liu, J.; Deng, Z.; Chen, L.-H.; Li, Y.; Su, B.-L., In-Situ Growing Mesoporous CuO/O-Doped g-C3N4 Nanospheres for Highly Enhanced Lithium Storage. *ACS Appl. Mater. Interfaces* **2019,** *11* (36), 32957-32968.

54. Wang, J.; Xu, H.; Qian, X.; Dong, Y.; Gao, J.; Qian, G.; Yao, J., Direct Synthesis of Porous Nanorod-Type Graphitic Carbon Nitride/CuO Composite from Cu–Melamine Supramolecular Framework towards Enhanced Photocatalytic Performance. *Chem. - Asian J.* **2015,** *10* (6), 1276-1280.

55. Zheng, W.; Li, Y.; Liu, M.; Tsang, C.-S.; Lee, L. Y. S.; Wong, K.-Y., Cu2+-doped Carbon Nitride/MWCNT as an Electrochemical Glucose Sensor. *Electroanalysis* **2018,** *30* (7), 1446-1454.

56. Fettkenhauer, C.; Wang, X. C.; Kailasam, K.; Antonietti, M.; Dontsova, D., Synthesis of efficient photocatalysts for water oxidation and dye degradation reactions using CoCl2 eutectics. *J. Mater. Chem. A* **2015,** *3* (42), 21227-21232.

57. Sridharan, K.; Kuriakose, T.; Philip, R.; Park, T. J., Transition metal (Fe, Co and Ni) oxide nanoparticles grafted graphitic carbon nitrides as efficient optical limiters and recyclable photocatalysts. *Appl. Surf. Sci.* **2014,** *308*, 139-147.

58. Sivasankaran, R. P.; Rockstroh, N.; Kreyenschulte, C. R.; Bartling, S.; Lund, H.; Acharjya, A.; Junge, H.; Thomas, A.; Brückner, A., Influence of MoS2 on Activity and Stability of Carbon Nitride in Photocatalytic Hydrogen Production *Catalysts* **2019,** *9* (8), 695-710.

59. Zhang, Y.; Li, K.; Liao, J.; Wei, X.; Zhang, L., Microwave-assisted synthesis of graphitic carbon nitride/CuO nanocomposites and the enhancement of catalytic activities in the thermal decomposition of ammonium perchlorate. *Appl. Surf. Sci.* **2020,** *499*, 143875.

60. Ngullie, R. C.; Alaswad, S. O.; Bhuvaneswari, K.; Shanmugam, P.; Pazhanivel, T.; Arunachalam, P., Synthesis and Characterization of Efficient ZnO/g-C(3)N(4)Nanocomposites Photocatalyst for Photocatalytic Degradation of Methylene Blue. *Coatings* **2020,** *10* (5), 14.

61. An, X. Q.; Hu, C. Z.; Lan, H. C.; Liu, H. J.; Qu, J. H., Strongly Coupled Metal Oxide/Reassembled Carbon Nitride/Co-Pi Heterostructures for Efficient Photoelectrochemical Water Splitting. *ACS Appl. Mater. Interfaces* **2018,** *10* (7), 6424-6432.

62. Liao, C.; Yang, B.; Zhang, N.; Liu, M.; Chen, G.; Jiang, X.; Chen, G.; Yang, J.; Liu, X.; Chan, T.-S.; Lu, Y.-J.; Ma, R.; Zhou, W., Constructing Conductive Interfaces between Nickel Oxide Nanocrystals and Polymer Carbon Nitride for Efficient Electrocatalytic Oxygen Evolution Reaction. *Adv. Funct. Mater.* **2019,** *29* (40), 1904020.

63. Tan, G. Q.; Wu, F.; Yuan, Y. F.; Chen, R. J.; Zhao, T.; Yao, Y.; Qian, J.; Liu, J. R.; Ye, Y. S.; Shahbazian-Yassar, R.; Lu, J.; Amine, K., Freestanding three-dimensional core-shell nanoarrays for lithium-ion battery anodes. *Nat. Commun.* **2016,** *7*, 10.

64. Sivasakthi, S.; Gurunathan, K., Graphitic carbon nitride bedecked with CuO/ZnO hetero-interface microflower towards high photocatalytic performance. *Renewable Energy* **2020,** *159*, 786-800.

65. Chai, B.; Peng, T.; Mao, J.; Li, K.; Zan, L., Graphitic carbon nitride (g-C3N4)–Pt-TiO2 nanocomposite as an efficient photocatalyst for hydrogen production under visible light irradiation. *Phys. Chem. Chem. Phys.* **2012,** *14* (48), 16745-16752.

66. He, L. H.; Cui, B. B.; Liu, J. M.; Wang, M. H.; Zhang, Z. H.; Zhang, H. Z., Fabrication of Porous CoOx/mC@MoS2 Composite Loaded on g-C3N4 Nanosheets as a Highly Efficient Dual Electrocatalyst for Oxygen Reduction and Hydrogen Evolution Reactions. *ACS Sustainable Chem. Eng.* **2018,** *6* (7), 9257-9268.

67. Zhang, D.; Gökce, B.; Barcikowski, S., Laser Synthesis and Processing of Colloids: Fundamentals and Applications. *Chemical Reviews* **2017,** *117* (5), 3990-4103.

68. Bohandy, J.; Kim, B. F.; Adrian, F. J., Metal-Deposition from a Supported Metal-Film Using an Excimer Laser. *J Appl Phys* **1986,** *60* (4), 1538-1539.

69. Pique, A.; Chrisey, D. B.; Auyeung, R. C. Y.; Fitz-Gerald, J.; Wu, H. D.; McGill, R. A.; Lakeou, S.; Wu, P. K.; Nguyen, V.; Duignan, M., A novel laser transfer process for direct writing of electronic and sensor materials. *Appl Phys a-Mater* **1999,** *69*, S279-S284.

70. Ringeisen, B. R.; Chrisey, D. B.; Pique, A.; Young, H. D.; Modi, R.; Bucaro, M.; Jones-Meehan, J.; Spargo, B. J., Generation of mesoscopic patterns of viable Escherichia coli by ambient laser transfer. *Biomaterials* **2002,** *23* (1), 161-166.

71. Kattamis, N. T.; Purnick, P. E.; Weiss, R.; Arnold, C. B., Thick film laser induced forward transfer for deposition of thermally and mechanically sensitive materials. *Appl Phys Lett* **2007,** *91* (17).

72. Banks, D. P.; Kaur, K.; Gazia, R.; Fardel, R.; Nagel, M.; Lippert, T.; Eason, R. W., Triazene photopolymer dynamic release layer-assisted femtosecond laser-induced forward transfer with an active carrier substrate. *Epl-Europhys Lett* **2008,** *83* (3).

73. Hecht, L.; Rager, K.; Davidonis, M.; Weber, P.; Gauglitz, G.; Dietzel, A., Blister-Actuated LIFT Printing for Multiparametric Functionalization of Paper-Like Biosensors. **2019**.

74. Palneedi, H.; Park, J. H.; Maurya, D.; Peddigari, M.; Hwang, G.-T.; Annapureddy, V.; Kim, J.-W.; Choi, J.-J.; Hahn, B.-D.; Priya, S.; Lee, K. J.; Ryu, J., Laser Irradiation of Metal Oxide Films and Nanostructures: Applications and Advances. *Adv. Mater.* **2018,** *30* (14), 1705148.

75. Arazoe, H.; Miyajima, D.; Akaike, K.; Araoka, F.; Sato, E.; Hikima, T.; Kawamoto, M.; Aida, T., An autonomous actuator driven by fluctuations in ambient humidity. *Nat. Mater.* **2016,** *15* (10), 1084-1089.

76. Bian, J.; Li, Q.; Huang, C.; Li, J.; Guo, Y.; Zaw, M.; Zhang, R.-Q., Thermal vapor condensation of uniform graphitic carbon nitride films with remarkable photocurrent density for photoelectrochemical applications. *Nano Energy* **2015,** *15*, 353-361.

77. Iijima, Y.; Niimura, N.; Hiraoka, K., Prevention of the Reduction of CuO during X-ray Photoelectron Spectroscopy Analysis. *Surface and Interface Analysis* **1996,** *24* (3), 193-197.

78. Gao, J.; Wang, J.; Qian, X.; Dong, Y.; Xu, H.; Song, R.; Yan, C.; Zhu, H.; Zhong, Q.; Qian, G.; Yao, J., One-pot synthesis of copper-doped graphitic carbon nitride nanosheet by heating Cu–melamine supramolecular network and its enhanced visible-light-driven photocatalysis. *J. Solid State Chem.* **2015,** *228*, 60-64.

79. Bafekry, A.; Stampfl, C.; Akgenc, B.; Ghergherehchi, M., Control of C3N4 and C4N3 carbon nitride nanosheets' electronic and magnetic properties through embedded atoms. *Physical Chemistry Chemical Physics* **2020,** *22* (4), 2249-2261.

80. Shrestha, K. M.; Sorensen, C. M.; Klabunde, K. J., Synthesis of CuO Nanorods, Reduction of CuO into Cu Nanorods, and Diffuse Reflectance Measurements of CuO and Cu Nanomaterials in the Near Infrared Region. *J. Phys. Chem. C* **2010,** *114* (34), 14368-14376.

81. Cheng, Z.; Xu, J.; Zhong, H.; Chu, X.; Song, J., Hydrogen peroxide-assisted hydrothermal synthesis of hierarchical CuO flower-like nanostructures. *Mater. Lett.* **2011,** *65* (13), 2047-2050.

82. Wan, M.; Jin, D.; Feng, R.; Si, L.; Gao, M.; Yue, L., Pillow-shaped porous CuO as anode material for lithium-ion batteries. *Inorg. Chem. Commun.* **2011,** *14* (1), 38-41.

83. Jiang, X.; Herricks, T.; Xia, Y., CuO Nanowires Can Be Synthesized by Heating Copper Substrates in Air. *Nano Lett.* **2002,** *2* (12), 1333-1338.

84. Chawla, M.; Sharma, V.; Randhawa, J. K., Facile One Pot Synthesis of CuO Nanostructures and Their Effect on Nonenzymatic Glucose Biosensing. *Electrocatalysis* **2017,** *8* (1), 27-35.

85. Dar, M. A.; Ahsanulhaq, Q.; Kim, Y. S.; Sohn, J. M.; Kim, W. B.; Shin, H. S., Versatile synthesis of rectangular shaped nanobat-like CuO nanostructures by hydrothermal method; structural properties and growth mechanism. *Appl. Surf. Sci.* **2009,** *255* (12), 6279-6284.

86. Sun, S.; Zhang, X.; Zhang, J.; Wang, L.; Song, X.; Yang, Z., Surfactant-free CuO mesocrystals with controllable dimensions: green ordered-aggregation-driven synthesis, formation mechanism and their photochemical performances. *CrystEngComm* **2013,** *15* (5), 867-877.

87. Qiu, G.; Dharmarathna, S.; Zhang, Y.; Opembe, N.; Huang, H.; Suib, S. L., Facile Microwave-Assisted Hydrothermal Synthesis of CuO Nanomaterials and Their Catalytic and Electrochemical Properties. *J. Phys. Chem. C* **2012,** *116* (1), 468-477.

88. Eickelmann, S.; Ronneberger, S.; Zhang, J.; Paris, G.; Loeffler, F. F., Alkanes as Intelligent Surface Thermometers: A Facile Approach to Characterize Short-Lived Temperature Gradients on the Micrometer Scale. *Advanced Materials Interfaces n/a* (n/a), 2001626.

89. Zhang, J.; Gim, S.; Paris, G.; Dallabernardina, P.; Schmitt, C. N. Z.; Eickelmann, S.; Loeffler, F. F., Ultrasonic-Assisted Synthesis of Highly Defined Silver Nanodimers by Self-Assembly for Improved Surface-Enhanced Raman Spectroscopy. *Chem. - Eur. J.* **2020,** *26* (6), 1243-1248.

90. Liu, B.; Zeng, H. C., Mesoscale organization of CuO nanoribbons: Formation of "dandelions". *J. Am. Chem. Soc.* **2004,** *126* (26), 8124-8125.

91. Zhang, Q.; Liu, S. J.; Yu, S. H., Recent advances in oriented attachment growth and synthesis of functional materials: Concept, evidence, mechanism, and future. *J. Mater. Chem.* **2009,** *19* (2), 191-207.

92. Zhang, Z.; Sun, H.; Shao, X.; Li, D.; Yu, H.; Han, M., Three-Dimensionally Oriented Aggregation of a Few Hundred Nanoparticles into Monocrystalline Architectures. *Adv. Mater.* **2005,** *17* (1), 42-47.

93. Zhang, W.; Wen, X.; Yang, S.; Berta, Y.; Wang, Z. L., Single-crystalline scroll-type nanotube arrays of copper hydroxide synthesized at room temperature. *Adv. Mater.* **2003,** *15* (10), 822-825.

94. Zhang, Q.; Zhang, K.; Xu, D.; Yang, G.; Huang, H.; Nie, F.; Liu, C.; Yang, S., CuO nanostructures: Synthesis, characterization, growth mechanisms, fundamental properties, and applications. *Prog. Mater. Sci.* **2014,** *60*, 208-337.

95. Li, Y.; Gu, M.; Zhang, X.; Fan, J.; Lv, K.; Carabineiro, S. A. C.; Dong, F., 2D g-C3N4 for advancement of photo-generated carrier dynamics: Status and challenges. *Materials Today* **2020,** *41*, 270-303.

96. Dong, G.; Zhao, K.; Zhang, L., Carbon self-doping induced high electronic conductivity and photoreactivity of g-C3N4. *Chemical Communications* **2012,** *48* (49), 6178-6180.

97. Huang, Z.-F.; Song, J.; Pan, L.; Wang, Z.; Zhang, X.; Zou, J.-J.; Mi, W.; Zhang, X.; Wang, L., Carbon nitride with simultaneous porous network and O-doping for efficient solar-energy-driven hydrogen evolution. *Nano Energy* **2015,** *12*, 646-656.

98. Li, Y.; Wang, S.; Chang, W.; Zhang, L.; Wu, Z.; Song, S.; Xing, Y., Preparation and enhanced photocatalytic performance of sulfur doped terminal-methylated g-C3N4 nanosheets with extended visible-light response. *Journal of Materials Chemistry A* **2019,** *7* (36), 20640-20648.

99. Pan, J.; Liu, G.; Lu, G. Q.; Cheng, H.-M., On the True Photoreactivity Order of {001}, {010}, and {101} Facets of Anatase TiO2 Crystals. *Angewandte Chemie International Edition* **2011,** *50* (9), 2133-2137.

100. Li, L.; Salvador, P. A.; Rohrer, G. S., Photocatalysts with internal electric fields. *Nanoscale* **2014,** *6* (1), 24-42.

101. Peng, G.; Volokh, M.; Tzadikov, J.; Sun, J.; Shalom, M., Carbon Nitride/Reduced Graphene Oxide Film with Enhanced Electron Diffusion Length: An Efficient Photo-Electrochemical Cell for Hydrogen Generation. *Adv. Energy Mater.* **2018,** *8* (23), 1800566.

102. Ruan, Q.; Luo, W.; Xie, J.; Wang, Y.; Liu, X.; Bai, Z.; Carmalt, C. J.; Tang, J., A Nanojunction Polymer Photoelectrode for Efficient Charge Transport and Separation. *Angew. Chem., Int. Ed.* **2017,** *56* (28), 8221-8225.

103. Fang, Y.; Li, X.; Wang, X., Synthesis of Polymeric Carbon Nitride Films with Adhesive Interfaces for Solar Water Splitting Devices. *ACS Catal.* **2018,** *8* (9), 8774-8780.

104. Luan, P.; Meng, Q.; Wu, J.; Li, Q.; Zhang, X.; Zhang, Y.; O'Dell, L. A.; Raga, S. R.; Pringle, J.; Griffith, J. C.; Sun, C.; Bach, U.; Zhang, J., Unique Layer-Doping-Induced Regulation of Charge Behavior in Metal-Free Carbon Nitride Photoanodes for Enhanced Performance. *ChemSusChem* **2020,** *13* (2), 328-333.

105. Zhao, T.; Zhou, Q.; Lv, Y.; Han, D.; Wu, K.; Zhao, L.; Shen, Y.; Liu, S.; Zhang, Y., Ultrafast Condensation of Carbon Nitride on Electrodes with Exceptional Boosted Photocurrent and Electrochemiluminescence. *Angew. Chem., Int. Ed.* **2020,** *59* (3), 1139-1143.

106. Zhang, W.; Albero, J.; Xi, L.; Lange, K. M.; Garcia, H.; Wang, X.; Shalom, M., One-Pot Synthesis of Nickel-Modified Carbon Nitride Layers Toward Efficient Photoelectrochemical Cells. *ACS Appl. Mater. Interfaces* **2017,** *9* (38), 32667-32677.

107. Yang, L.; Zhao, Z.; Hu, J.; Wang, H.; Dong, J.; Wan, X.; Cai, Z.; Li, M., Copper Oxide Nanoparticles with Graphitic Carbon Nitride for Ultrasensitive

Photoelectrochemical Aptasensor of Bisphenol A. *Electroanalysis* **2020,** *32* (7), 1651-1658.

108. Liu, Y.; Yu, Y.-X.; Zhang, W.-D., Photoelectrochemical study on charge transfer properties of nanostructured Fe2O3 modified by g-C3N4. *International Journal of Hydrogen Energy* **2014,** *39* (17), 9105-9113.

109. Hou, Y.; Wen, Z.; Cui, S.; Feng, X.; Chen, J., Strongly Coupled Ternary Hybrid Aerogels of N-deficient Porous Graphitic-C3N4 Nanosheets/N-Doped Graphene/NiFe-Layered Double Hydroxide for Solar-Driven Photoelectrochemical Water Oxidation. *Nano Letters* **2016,** *16* (4), 2268-2277.

110. Ni, M.; Leung, M. K. H.; Leung, D. Y. C.; Sumathy, K., A review and recent developments in photocatalytic water-splitting using TiO2 for hydrogen production. *Renewable and Sustainable Energy Reviews* **2007,** *11* (3), 401-425.

111. Zhang, Y.; Liu, Y.; Su, L.; Zhang, Z.; Huo, D.; Hou, C.; Lei, Y., CuO nanowires based sensitive and selective non-enzymatic glucose detection. *Sens. Actuators, B* **2014,** *191*, 86-93.

112. Zhao, Y.; Bo, X.; Guo, L., Highly exposed copper oxide supported on three-dimensional porous reduced graphene oxide for non-enzymatic detection of glucose. *Electrochim. Acta* **2015,** *176*, 1272-1279.

113. Xu, W.; Dai, S.; Wang, X.; He, X.; Wang, M.; Xi, Y.; Hu, C., Nanorod-aggregated flower-like CuO grown on a carbon fiber fabric for a super high sensitive non-enzymatic glucose sensor. *J. Mater. Chem. B* **2015,** *3* (28), 5777-5785.

114. Rahim, A.; Rehman, Z. U.; Mir, S.; Muhammad, N.; Rehman, F.; Nawaz, M. H.; Yaqub, M.; Siddiqi, S. A.; Chaudhry, A. A., A non-enzymatic glucose sensor based on CuO-nanostructure modified carbon ceramic electrode. *J. Mol. Liq.* **2017,** *248*, 425-431.

115. Sridara, T. U., J.; Saianand, G.; Tuantranont, A.; Karuwan, C.; Jakmunee, J., Non-Enzymatic Amperometric Glucose Sensor Based on Carbon Nanodots and Copper Oxide Nanocomposites Electrode. *Sensors* **2020,** *20*, 808.

116. Zhou, Z.; Zhu, Z.; Cui, F.; Shao, J.; Zhou, H. S., CuO/Cu composite nanospheres on a TiO2 nanotube array for amperometric sensing of glucose. *Microchim. Acta* **2020,** *187* (2), 123.

117. Cao, L.; Wang, P.; Chen, L.; Wu, Y.; Di, J., A photoelectrochemical glucose sensor based on gold nanoparticles as a mimic enzyme of glucose oxidase. *RSC Advances* **2019,** *9* (27), 15307-15313.

118. Devadoss, A.; Sudhagar, P.; Das, S.; Lee, S. Y.; Terashima, C.; Nakata, K.; Fujishima, A.; Choi, W.; Kang, Y. S.; Paik, U., Synergistic Metal–Metal Oxide Nanoparticles Supported Electrocatalytic Graphene for Improved Photoelectrochemical Glucose Oxidation. *ACS Applied Materials & Interfaces* **2014,** *6* (7), 4864-4871.

119. Zhang, X.; Xu, F.; Zhao, B.; Ji, X.; Yao, Y.; Wu, D.; Gao, Z.; Jiang, K., Synthesis of CdS quantum dots decorated graphene nanosheets and non-enzymatic photoelectrochemical detection of glucose. *Electrochimica Acta* **2014,** *133*, 615-622.

120. Wang, S.; Li, S.; Wang, W.; Zhao, M.; Liu, J.; Feng, H.; Chen, Y.; Gu, Q.; Du, Y.; Hao, W., A non-enzymatic photoelectrochemical glucose sensor based on BiVO4 electrode under visible light. *Sensors and Actuators B: Chemical* **2019,** *291*, 34-41.

121. Zhimin Ma, S. L., A Novel Photoelectrochemical Glucose Sensor Based on Graphene-CdS Nanocomposites Decorated with CoOx Nanosheets. *Int. J. Electrochem. Sci.* **2019,** *14*, 11445–11455.

122. Tobaldi, D. M.; Espro, C.; Leonardi, S. G.; Lajaunie, L.; Seabra, M. P.; Calvino, J. J.; Marini, S.; Labrincha, J. A.; Neri, G., Photo-electrochemical properties of CuO–TiO2 heterojunctions for glucose sensing. *Journal of Materials Chemistry C* **2020,** *8* (28), 9529-9539.

123. Ahmad, R.; Tripathy, N.; Ahn, M.-S.; Bhat, K. S.; Mahmoudi, T.; Wang, Y.; Yoo, J.-Y.; Kwon, D.-W.; Yang, H.-Y.; Hahn, Y.-B., Highly Efficient Non-Enzymatic Glucose Sensor Based on CuO Modified Vertically-Grown ZnO Nanorods on Electrode. *Scientific Reports* **2017,** *7* (1), 5715.

124. Li, X. H.; Antonietti, M., Metal nanoparticles at mesoporous N-doped carbons and carbon nitrides: functional Mott-Schottky heterojunctions for catalysis. *Chemical Society Reviews* **2013,** *42* (16), 6593-6604.

125. Wang, L.; Wang, C.; Hu, X.; Xue, H.; Pang, H., Metal/Graphitic Carbon Nitride Composites: Synthesis, Structures, and Applications. *Chemistry – An Asian Journal* **2016,** *11* (23), 3305-3328.

126. Yang, Y.; Guo, Y.; Liu, F.; Yuan, X.; Guo, Y.; Zhang, S.; Guo, W.; Huo, M., Preparation and enhanced visible-light photocatalytic activity of silver deposited graphitic carbon nitride plasmonic photocatalyst. *Applied Catalysis B: Environmental* **2013,** *142-143*, 828-837.

127. Li, Z.; Wang, J.; Zhu, K.; Ma, F.; Meng, A., Ag/g-C3N4 composite nanosheets: Synthesis and enhanced visible photocatalytic activities. *Materials Letters* **2015,** *145*, 167-170.

128. Xue, J.; Ma, S.; Zhou, Y.; Zhang, Z.; He, M., Facile Photochemical Synthesis of Au/Pt/g-C3N4 with Plasmon-Enhanced Photocatalytic Activity for Antibiotic Degradation. *ACS Applied Materials & Interfaces* **2015,** *7* (18), 9630-9637.

129. Yoo, I.-h.; Kalanur, S. S.; Seo, H., A nanoscale p–n junction photoelectrode consisting of an NiOx layer on a TiO2/CdS nanorod core-shell structure for highly efficient solar water splitting. *Applied Catalysis B: Environmental* **2019,** *250*, 200-212.

130. Yoo, I.-h.; Kalanur, S. S.; Seo, H., A nanoscale p–n junction photoelectrode consisting of an NiOx layer on a TiO2/CdS nanorod core-shell structure for highly efficient solar water splitting. *Appl. Catal., B* **2019,** *250*, 200-212.

131. Buscema, M.; Groenendijk, D. J.; Steele, G. A.; van der Zant, H. S. J.; Castellanos-Gomez, A., Photovoltaic effect in few-layer black phosphorus PN junctions defined by local electrostatic gating. *Nat. Commun.* **2014,** *5* (1), 4651.

132. Sawicka-Chudy, P.; Sibiński, M.; Wisz, G.; Rybak-Wilusz, E.; Cholewa, M., Numerical analysis and optimization of Cu2O/TiO2, CuO/TiO2, heterojunction solar cells using SCAPS. *Journal of Physics: Conference Series* **2018,** *1033*, 012002.

133. Alam, K. M.; Kumar, P.; Kar, P.; Thakur, U. K.; Zeng, S.; Cui, K.; Shankar, K., Enhanced charge separation in g-C3N4–BiOI heterostructures for visible light driven photoelectrochemical water splitting. *Nanoscale Adv.* **2019,** *1* (4), 1460-1471.

134. Ye, K.-H.; Li, H.; Huang, D.; Xiao, S.; Qiu, W.; Li, M.; Hu, Y.; Mai, W.; Ji, H.; Yang, S., Enhancing photoelectrochemical water splitting by combining work function tuning and heterojunction engineering. *Nat. Commun.* **2019,** *10* (1), 3687.

135. Franz, J. F.; Kraus, W. B.; Zeitler, K., No photocatalyst required – versatile, visible light mediated transformations with polyhalomethanes. *Chemical Communications* **2015,** *51* (39), 8280-8283.

Appendix 1: NMR spectra

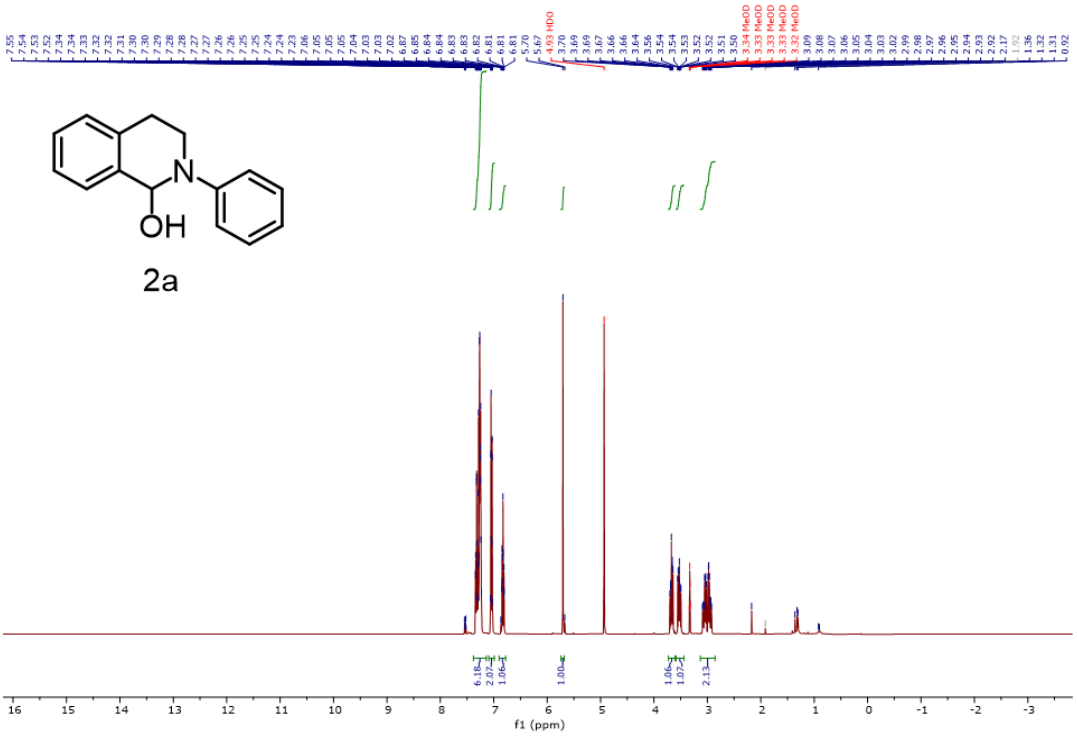

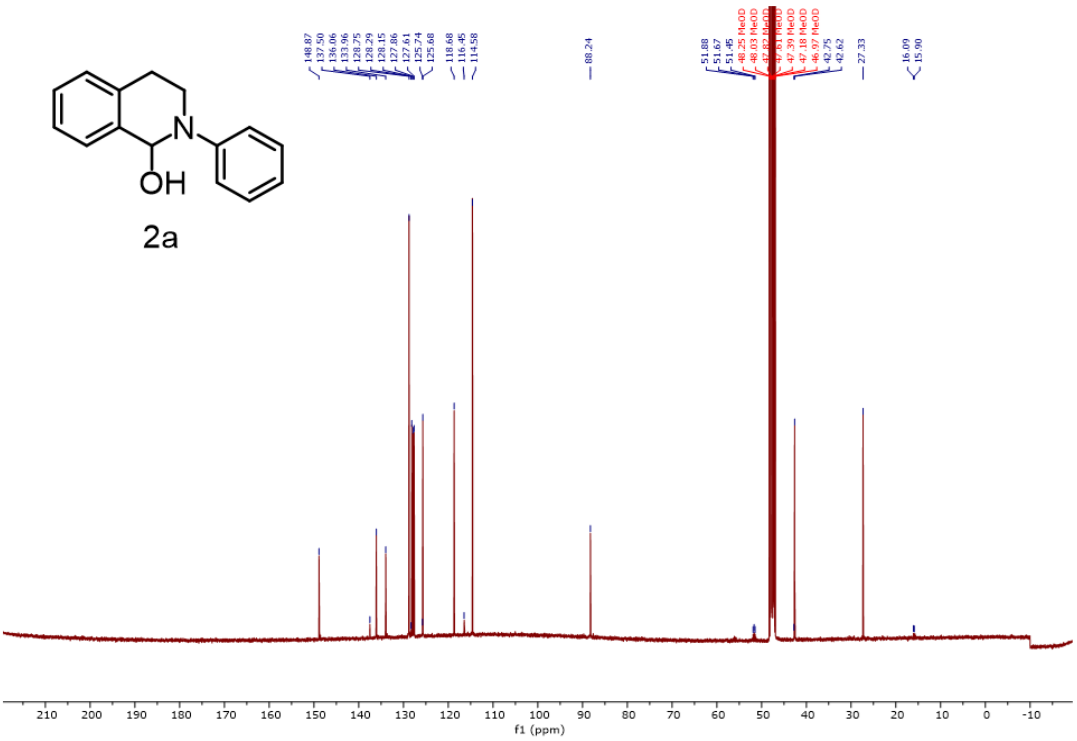

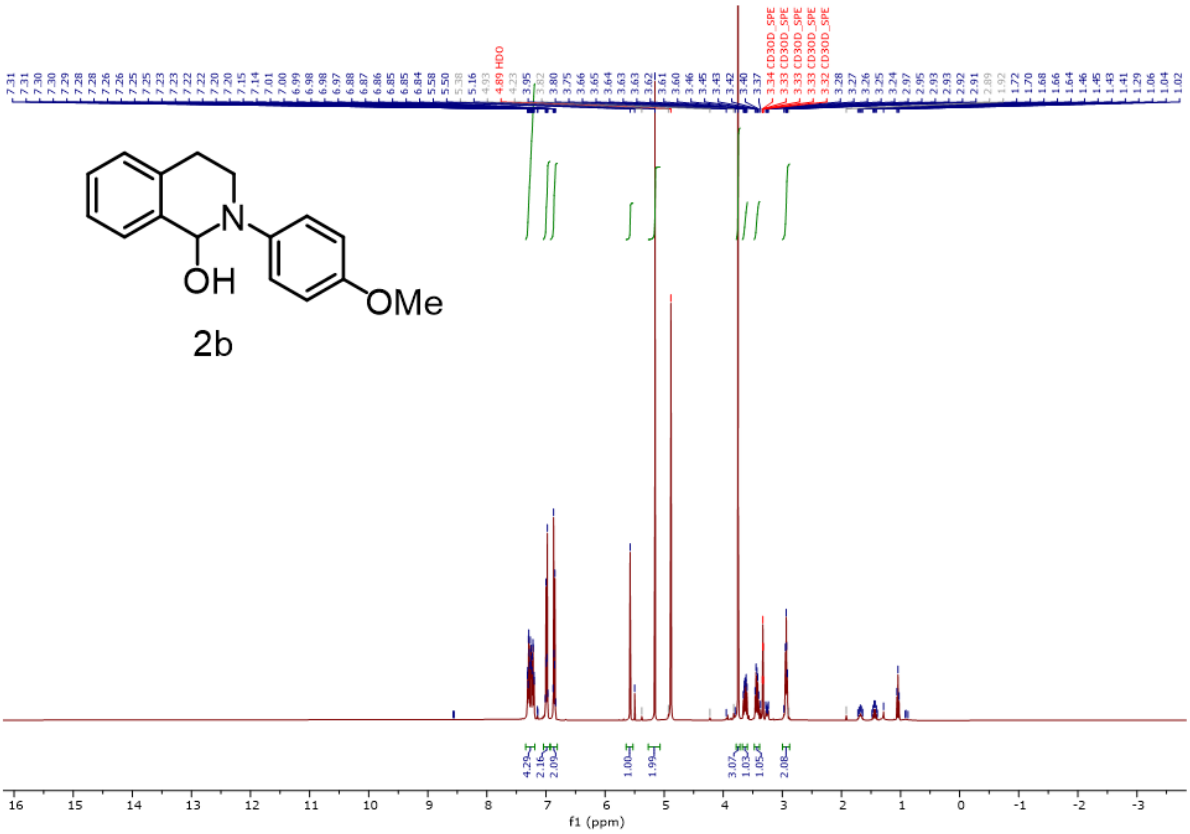
OH
N
OMe
2b
f1 (ppm)

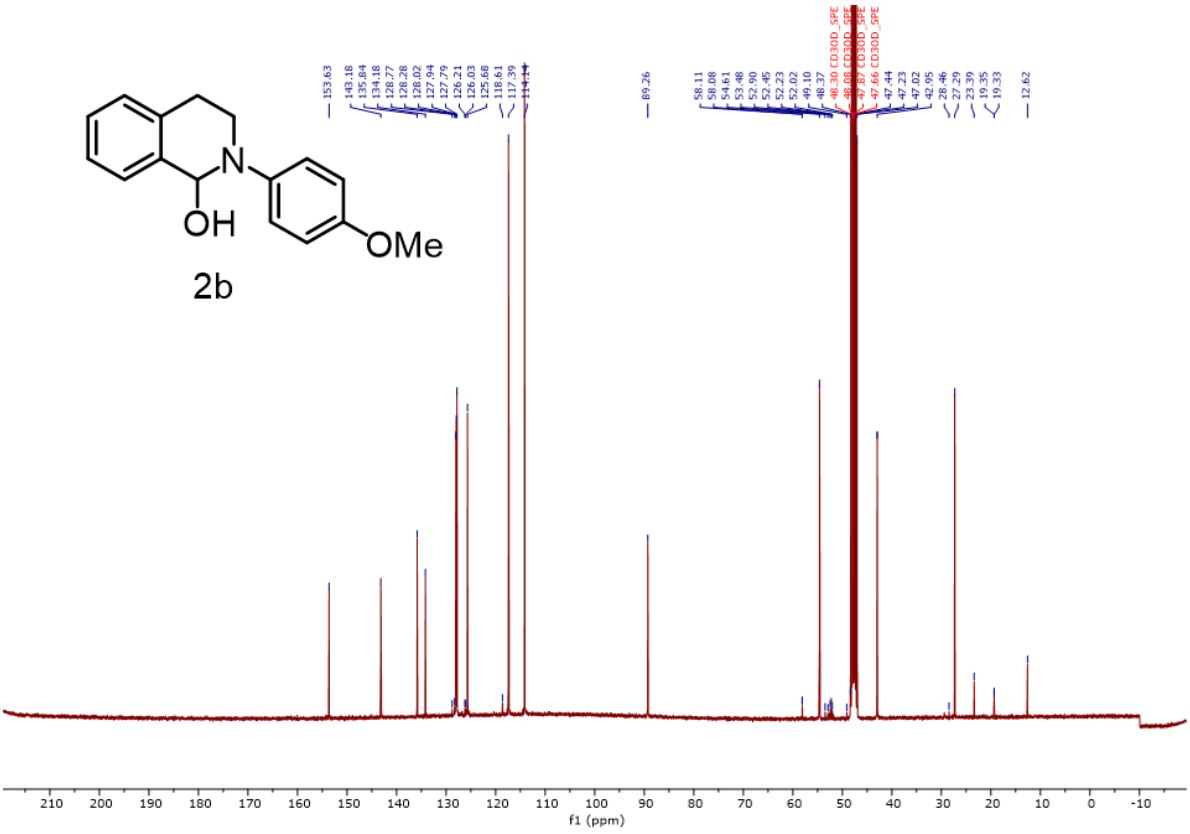
OH
N
OMe
2b
f1 (ppm)

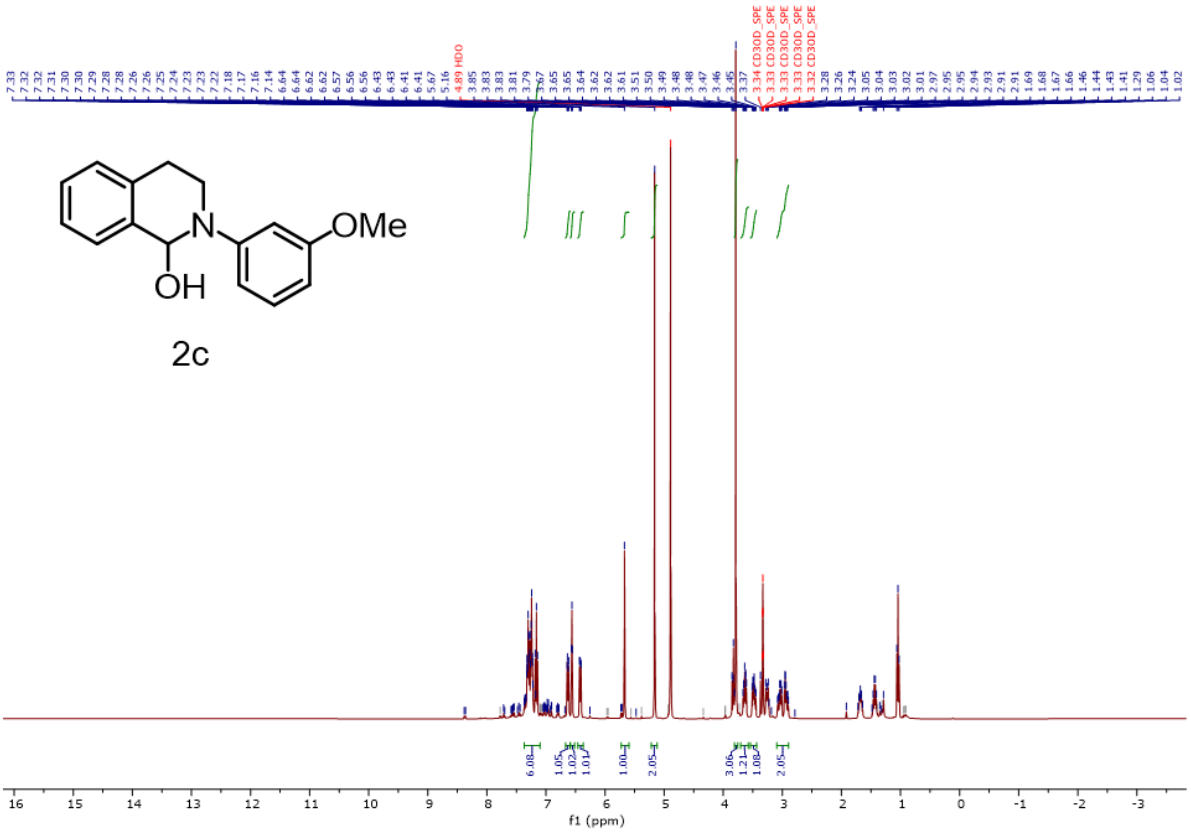
OMe
OH
2c
f1 (ppm)

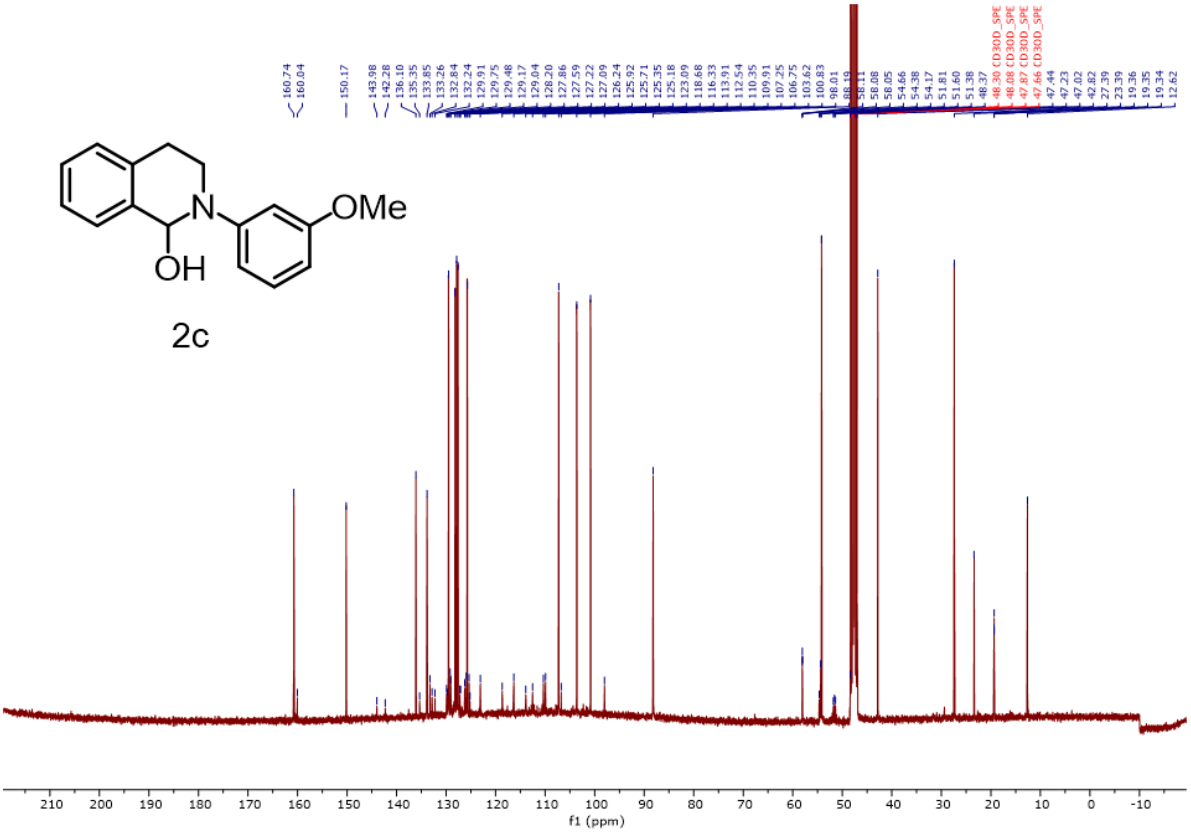
OMe
OH
2c
f1 (ppm)

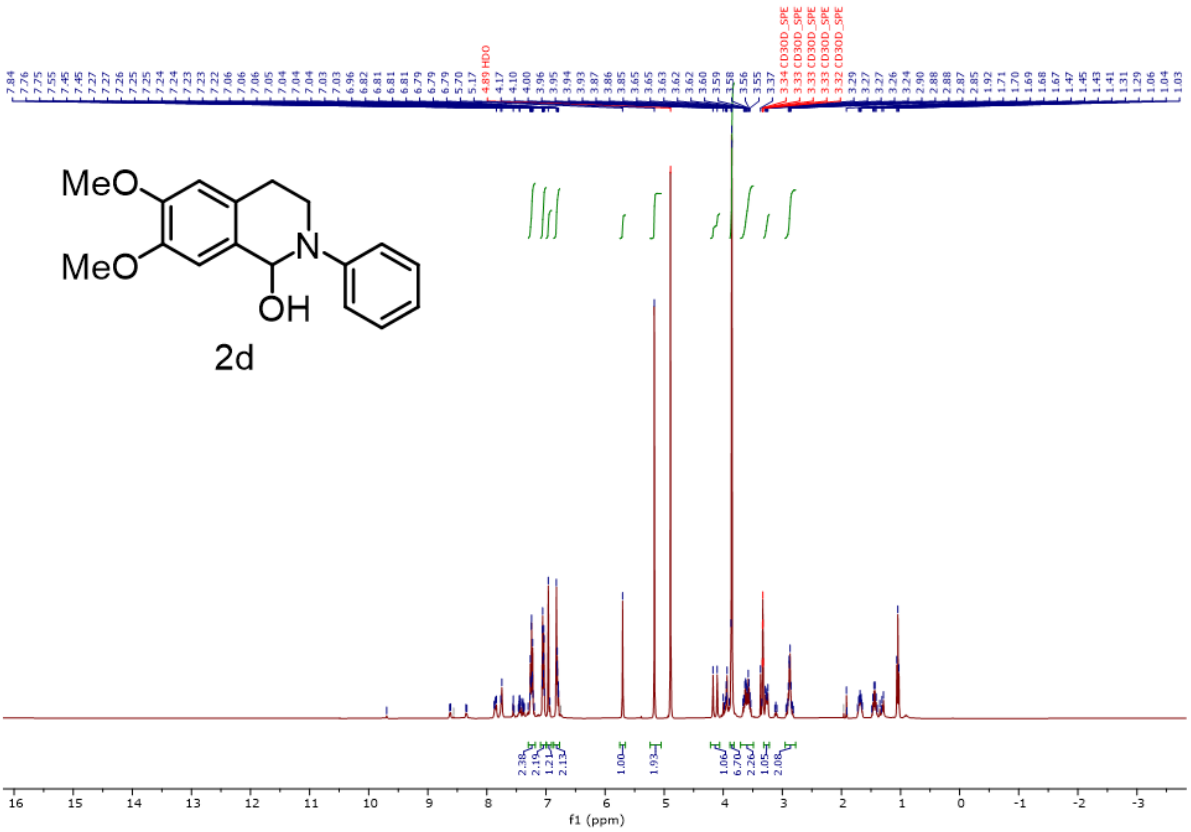
MeO
MeO
N
OH
2d
f1 (ppm)

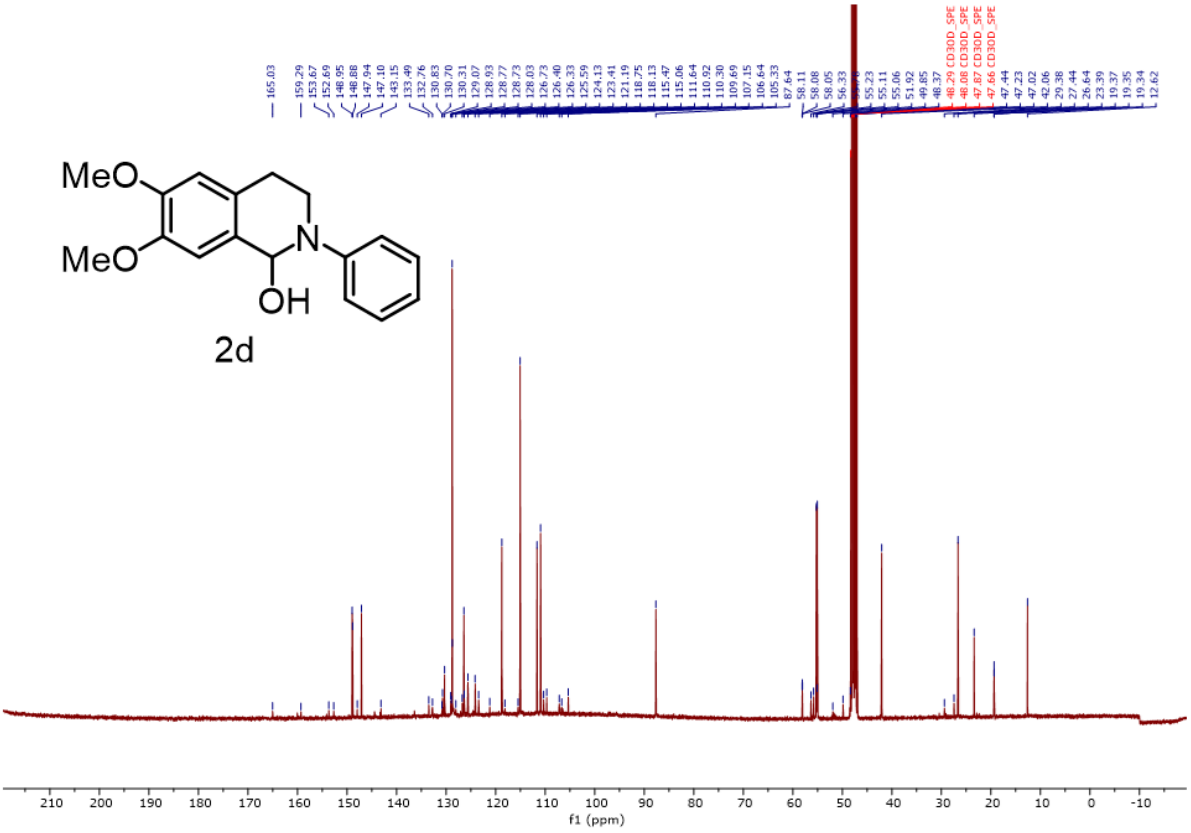
MeO
MeO
N
OH
2d
f1 (ppm)

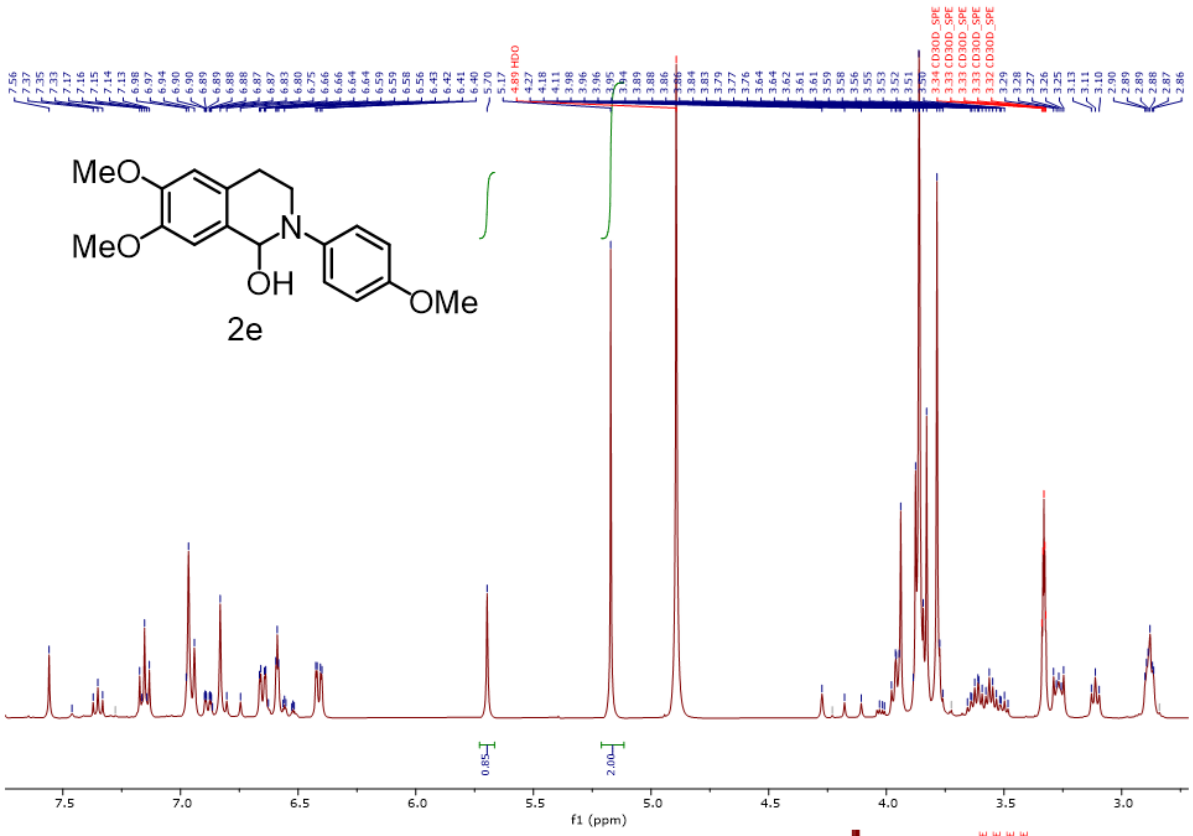
MeO
MeO
N
OH
OMe
2e
f1 (ppm)

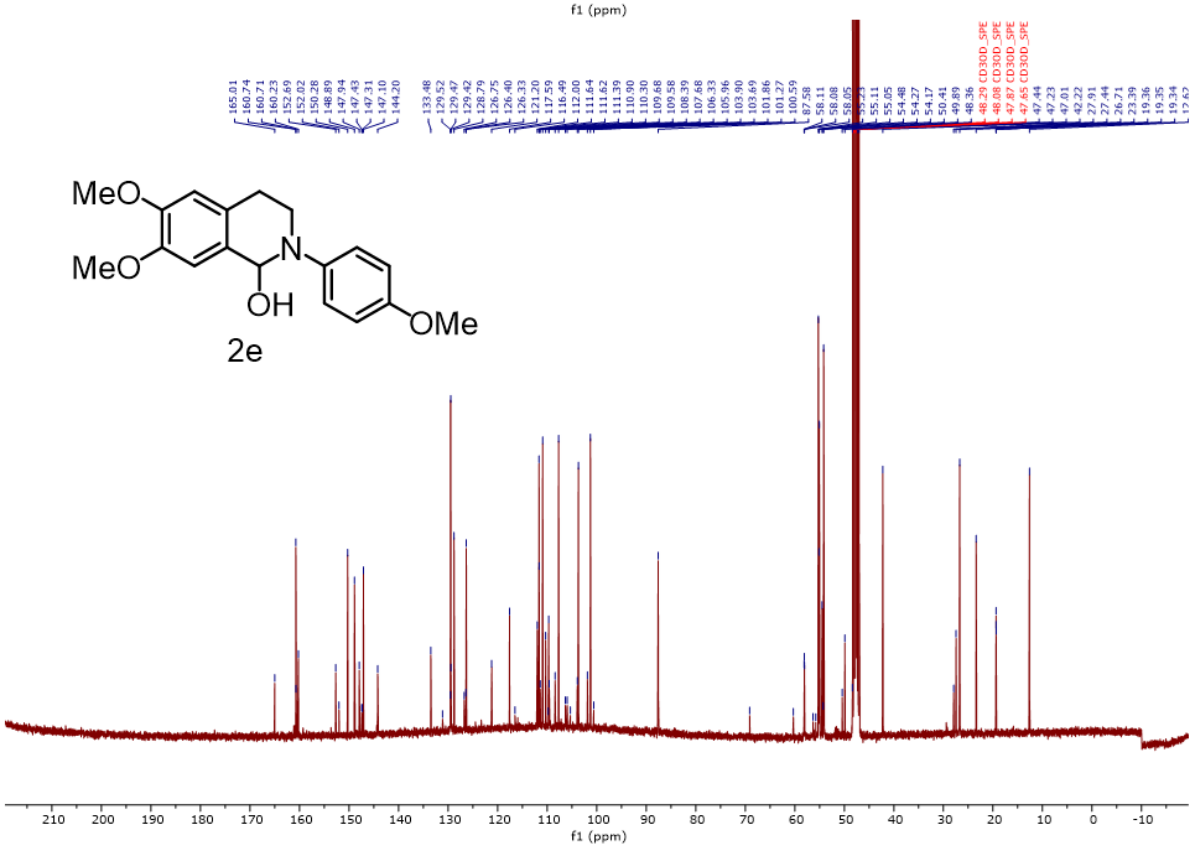
MeO
MeO
N
OH
OMe
2e
f1 (ppm)

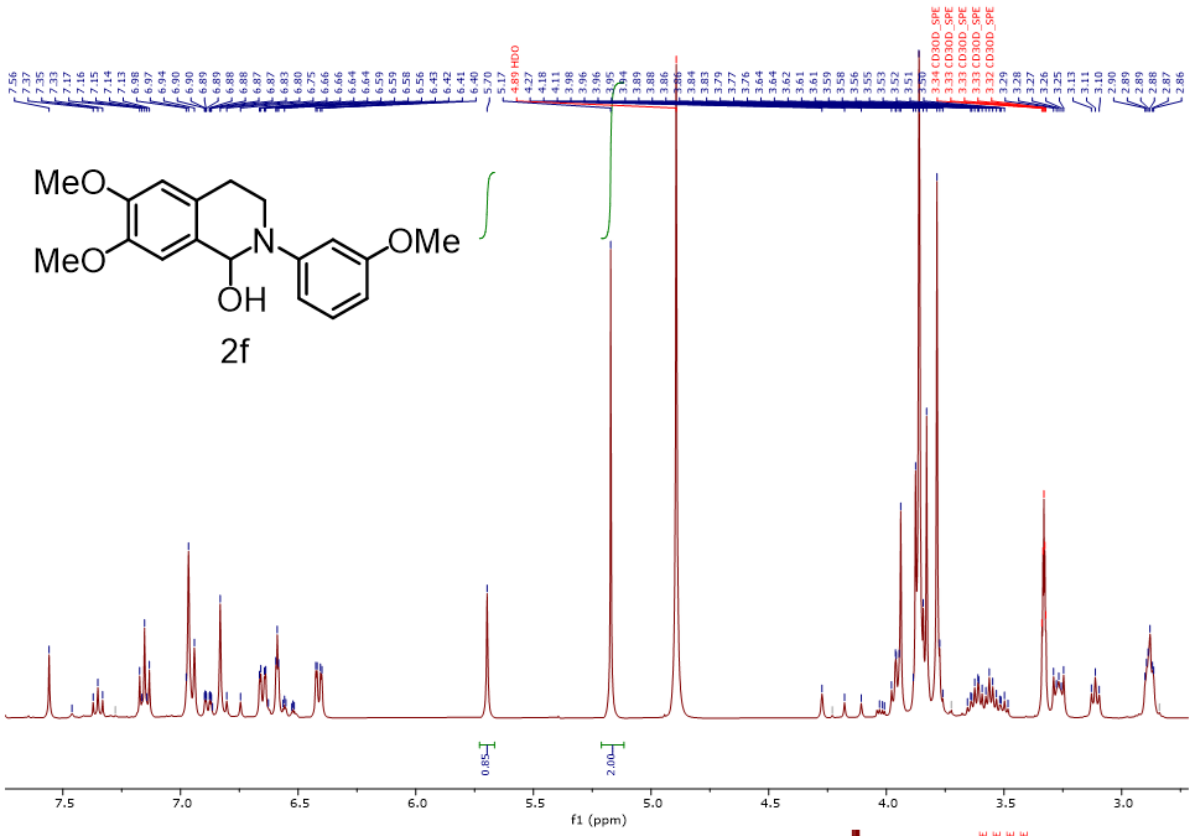
MeO
MeO
N
OMe
OH
2f
f1 (ppm)

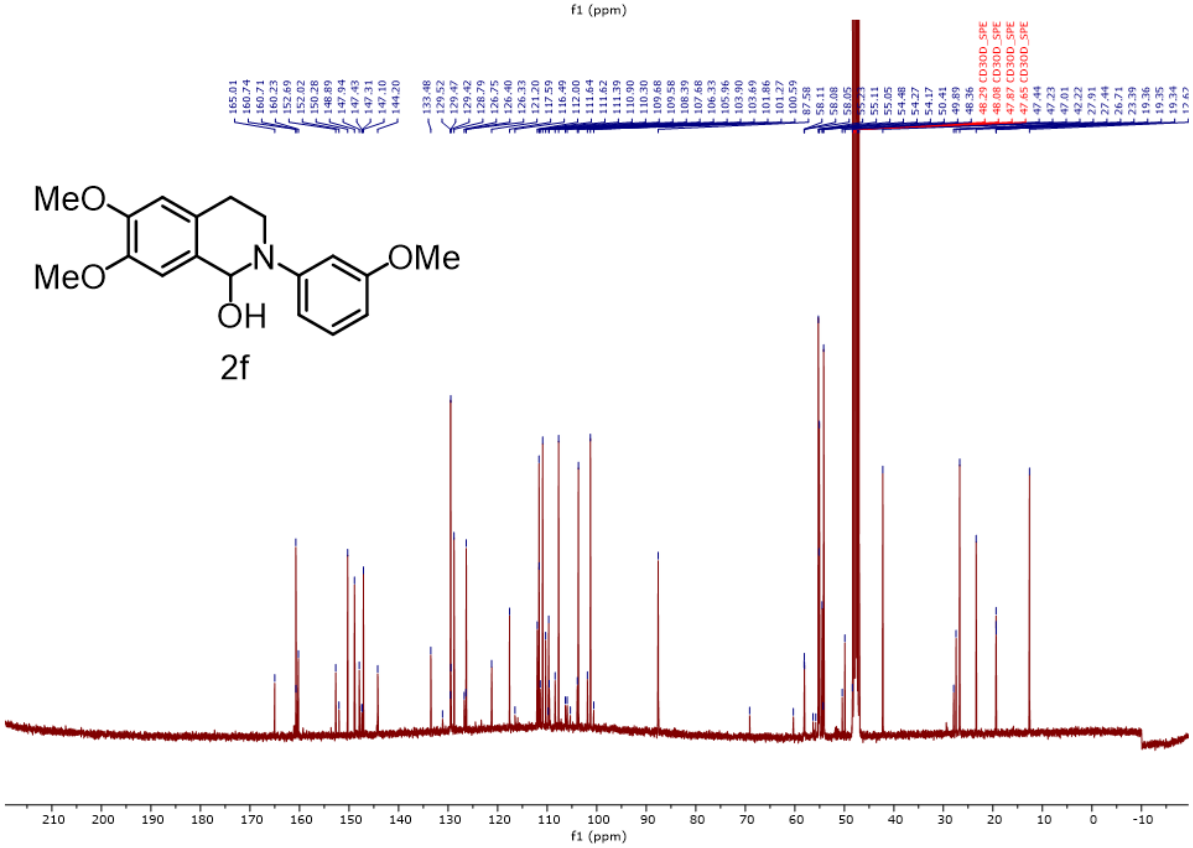
MeO
MeO
N
OMe
OH
2f
f1 (ppm)

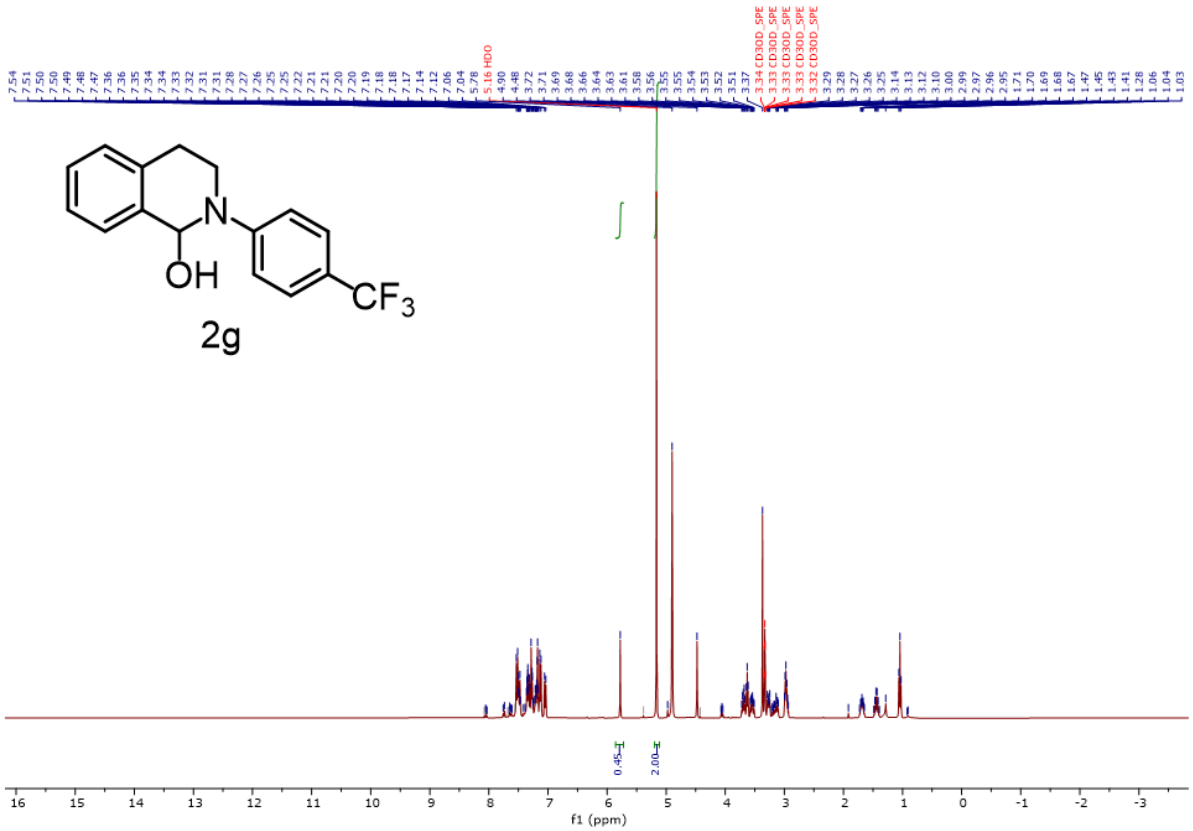
OH
CF3
2g
f1 (ppm)

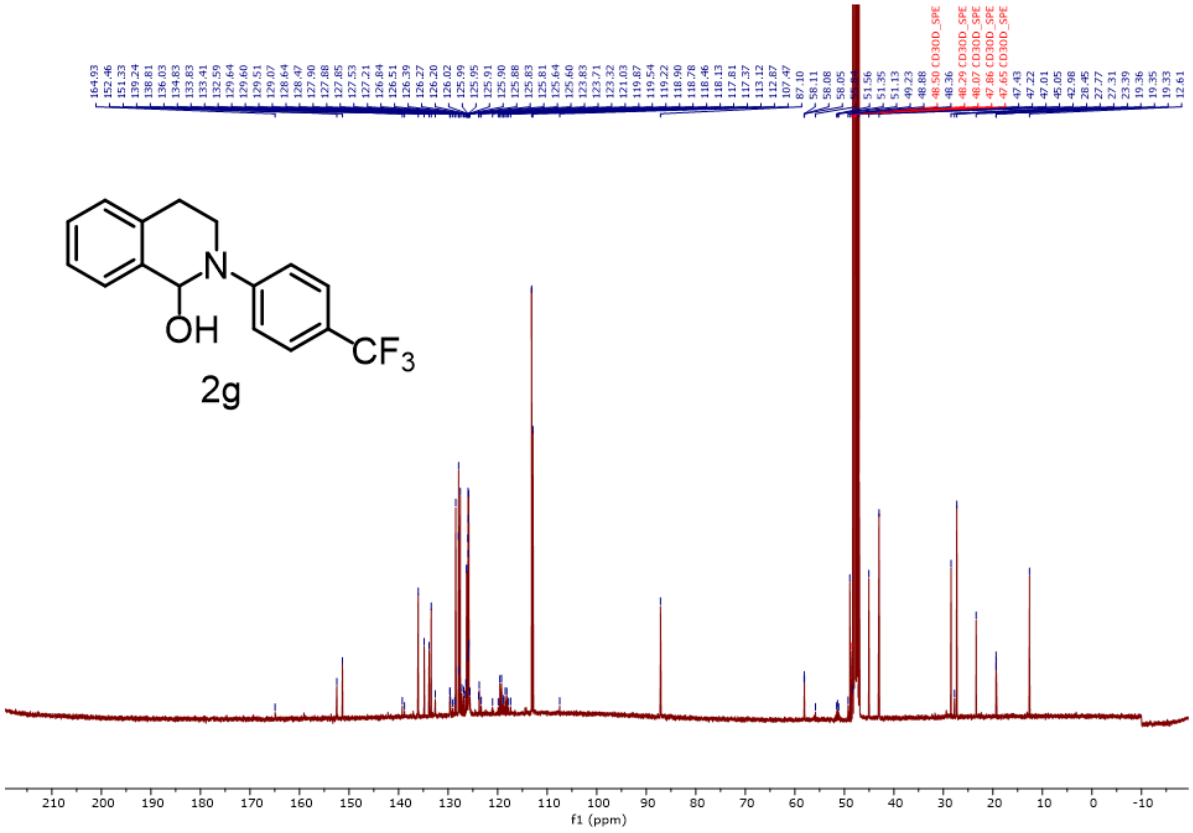
OH
CF3
2g
f1 (ppm)